Cavitation formation and modelling for fluid film bearings: A review

M J Braun and W M Hannon

Proceedings of the Institution of Mechanical Engineers, Part J: Journal of Engineering Tribology 2010 224: 839
DOI: 10.1243/13506501JET772

Cavitation formation and modelling for fluid film bearings: a review

M J Braun[1]* and **W M Hannon**[2]
[1]Department of Mechanical Engineering, University of Akron, Akron, OH, USA
[2]The Timken Company, Canton, Ohio, USA

The manuscript was received on 10 December 2009 and was accepted after revision for publication on 11 May 2010.

DOI: 10.1243/13506501JET772

Abstract: Even though the list of references associated with this review is rather extensive, in no way does it exhaust the vast literature dedicated to the study of cavitation. The intent was to summarize (i) advances in analytical and numerical modelling, (ii) draw attention to the thermodynamic aspects of cavitation, and (iii) do so while reflecting on physical or experimental observations.

Keywords: gaseous cavitation, vaporous cavitation, pseudo cavitation, hydrodynamic bearing cavitation

1 INTRODUCTION

The three recognized forms of liquid cavitation are reviewed in this article as follows.

1. 'Gaseous cavitation' generally contains one or multiple species of gases dissolved in the fluid and occurs as the pressure falls below the saturation pressure of the particular gas component.
2. 'Pseudo-cavitation' is a form of gaseous cavitation during which the gas bubble expands on account of depressurization without further gas mass diffusion from the liquid to the gas phase.
3. 'Vaporous cavitation' is the result of a thermodynamic non-equilibrium event when the pressure falls below the vapour pressure of the liquid at the prevalent temperature.

Osborne Reynolds [**1**] in his landmark paper of 1886 investigated the case of two cylindrical bearing surfaces operating eccentrically with respect to each other. His analysis was limited to lower eccentricities, ($\varepsilon < 0.5$), since he realized that it was doubtful that physically the fluid-film would sustain pressures below the atmospheric level. Due to the mathematical and computational complexities involved, the possibility of a film rupture and its implications to the overall static and dynamic behaviour of the bearing were not contemplated, nor could have been considered at that time. The result was the now famous Reynolds equation which is used to simulate an uninterrupted film around the bearing (Fig. 1(a)). In 1904, Sommerfeld [**2**] implemented a trigonometric substitution, henceforward known as the Sommerfeld transformation, which allows solutions of the Reynolds equation for all eccentricities and yields the now equally famous full Sommerfeld curve (Fig. 1(b)). The most notable feature of this curve is its negative anti-symmetric pressure in the divergent region of the bearing. Nominally, according to the Sommerfeld model, the minimum negative pressure is equal to the maximum positive one. For this model to be correct, the working fluid is assumed to be able to sustain high tensile stresses. It has been known for quite some time [**3**, **4**] that a fluid under certain conditions can sustain elevated levels of tensile stresses. This, however, is not such a realistic expectation in a tribological environment where fluid flow conditions exhibit extreme tangential shear, high rates of heat dissipation, and possibly strongly forming sub-atmospheric pressures. These conditions result in a film rupture wherein the resulting cavity, filled by either gas, vapour or a mixture thereof, has to be factored into the ensuing model.

2 LITERATURE REVIEW

There is a wealth of literature on cavitation, whether it is gaseous or vaporous, whether representative of

*Corresponding author: Department of Mechanical Engineering, University of Akron, Akron, OH 44325-3903, USA.
email: mjbraun@uakron.edu

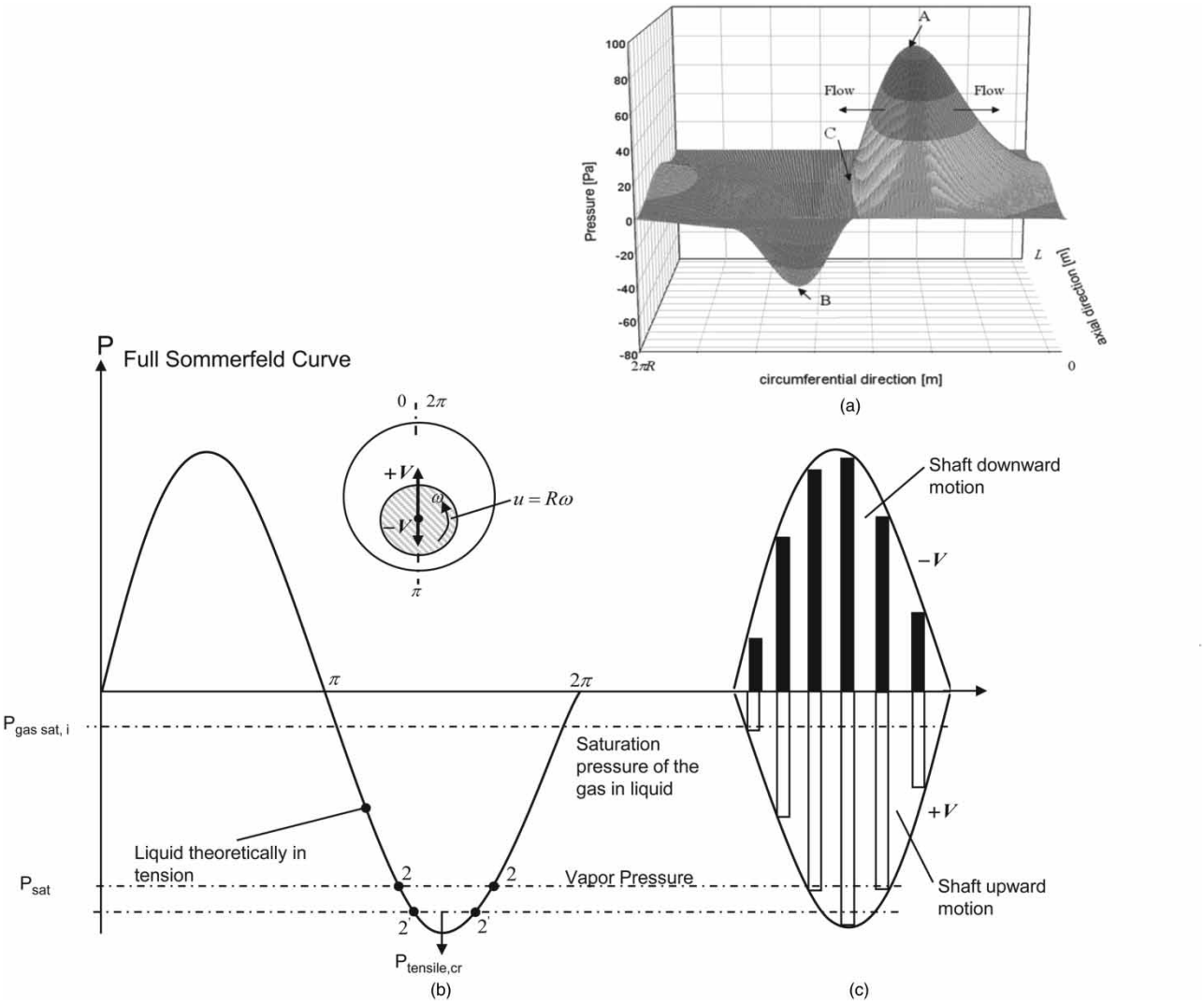

Fig. 1 Typical pressure distribution in a journal bearing with an eccentric shaft: (a) typical two-dimensional axial–circumferential pressure map distribution in a journal bearing; (b) 2D full Sommerfeld curve circumferential cross-section through the symmetry line of (a); and (c) typical circumferential pressure distribution in a convergent–divergent clearance with a normal velocity ±V to the main flow direction

sliding and/or rolling contacts or a fluid-film bearing subjected to dynamic loading (Figs 1(b) and (c)). In directing the interested reader to the richest literature wells regarding this subject, one has to acknowledge historically, across time, three symposia. The earliest modern era effort at gathering information about cavitation in one place is represented by a symposium organized by General Motors Research Labs in 1962 [**5**] and edited by Davies. Many of the participants in this symposium are today considered as forefathers in developing knowledge about bubble dynamics [**6**, **7**], surface tension [**8**, **9**] and thin film rupture [**10**–**12**]. The 1974, 1st Leeds-Lyon Symposium, edited by Dowson *et al.* [**13**], was the first to focus singly on the topic of cavitation phenomena as it relates to lubrication technology. This volume contains information regarding the fundamentals of vaporous and gaseous cavitation, classical theories addressing film rupture conditions in static and dynamically loaded bearings, and research relating to cavitation damage.

The 1988 NASA Lewis Research Center (Cleveland, Ohio, USA) symposium regarding cavitating films, Brewe *et al.* [**14**] contained the most recent advances (at that time) regarding the fundamental concepts of cavitation as well as follow-up improved versions of models presented in 1974 in Lyon [**13**]. In particular, the 1988 symposium offered novel theoretical algorithms for a more realistic simulation and numerical implementation of cavitation.

2.1 Types of cavitation

Swales [**15**] identified four general types of cavitation that are mostly vaporous in nature. He noted

that these types of cavitation are generally short-lived transient phenomena where the cavitating bubble grows and collapses as a function of both its pressure environment and capability of the fluid to resist tensile stresses. The four types of cavitation noted by Swales are the following:

(a) travelling;
(b) fixed;
(c) vortex;
(d) vibratory.

With the exception of the vortex cavitation where vortices have a relatively long residence time, the remaining types of cavitation, especially the vibratory type, are transitory in nature with rather short time constants. As Swales [**15**] and Dowson and Taylor [**16**] remark, the (a), (b), and (d) types of cavities are rather unstable, short-lived, and mostly contain vapour. The authors further note that cavitation is usually stable when the cavity's contents are gaseous as opposed to vaporous.

The travelling cavity is a most interesting phenomenon as the cavity forms, grows, and then closes as observed by an Eulerian viewer on the ground. Xing [**17**] in 2009, experimentally presented a classical case of such travelling cavity for a two-phase squeeze film damper. Sun and Brewe [**18**] have experimentally studied static and dynamically loaded bearings. They reached the conclusion that two different formulae are necessary to characterize the time constants associated with the following:

(a) vapour flashing and filling a void;
(b) gas diffusing out of the oil.

They proposed a formula [**19**] for calculating the time constant for vaporous cavitation and found it to be of the order of 167×10^{-6} s. They also calculated the time constant necessary for filling a void with diffused gases and determined it to be of the order of $0.32 \times 10^{+6}$ s. These findings in effect support the contention of Swales [**15**] and Dowson and Taylor [**16**] that gaseous cavitation is a much more stable phenomenon. By comparing these time constants with the operational characteristics of a dynamically loaded bearing, they concluded that vaporous cavitation occurs predominantly during dynamic situations. Even though the time constant for gas diffusion is much larger than that of a transitory (flash) depressurization process, otherwise predominant occurrence of gaseous cavitation is mitigated by the presence of gas nuclei in the oil film, or in the roughness of the crevices of the solid boundaries. In this environment of high film shear and tensile stresses, the nuclei act as gaseous 'cavitation promoters'. It is well known that for most common gases found in the atmosphere the gas saturation pressure in a liquid is far above that of its vapour pressure, even though both are subatmospheric. So the question poses itself as to what is the type of the cavity content: gaseous or vaporous? The answer certainly depends upon a multitude of factors that act conjointly: whether the fluid under consideration is pure or a mixture, whether the process is steady-state and diffusion-dominated, or highly transitory and characterized by sudden strong depressurization. Thus, the cavitation content, depending on the process, can either be gaseous, vaporous, or a combination thereof. As noted by both Swales [**15**] and Dowson and Taylor [**16**, **20**], when large amounts of gas (air) are dissolved in the lubricating oil there is a wealth of cavitation-starting nuclei. Under hydrodynamic conditions where the pressures fall below the gas saturation pressure, the gas diffuses out of the oil creating a stable cavity. Sun and Brewe [**18**, **19**], Sun *et al.* [**21**], Jacobson and Hamrock [**22**, **23**], Jacobson [**24**], and Wilson [**25**] have all addressed the circumstances of the vaporous cavitation, based on visual observation of a highly transitory regime and/or typical pitting cavitation damage.

2.2 On tensile stress of liquids

In 1974, Temperley [**26**] reviewed the available experimental data and state-of-the-art theory regarding the tensile strength of liquids. He determined experimentally that three different situations of 'fluid-in-tension' could be identified as the following:

(a) static application of tension;
(b) 'once-only' pulse tension test;
(c) oscillating tension through acoustic means.

For all three categories, it has been proven that the fluid can sustain significant levels of tension. The tensile strength values obtained from the type (1) experiments are significantly higher than type (2); both type (1) and (2) give yet higher tensile values than type (3) experiments. For further reading, Temperley refers to two of his earlier papers [**27**, **28**] where he reviewed work and studied the behaviour of water subjected to 'tension'. He mentions that considerable differences (as much as 50 times) were observed in the values of critical tension when different methods like those of Bertholet [**3**] and Reynolds [**4**] were used. Temperley reported that if tension is applied statically, ordinary tap water containing small amounts of dissolved air can withstand tensions as high as 4.06 MPa (40 atm) while under conditions of near saturation with air, water was found to withstand tensions of only 0.61 MPa (6 atm). Fisher [**29**] affirms that a liquid under 'negative pressure' (tension) is in a metastable state where vapour bubbles appear spontaneously and continue growing until the system's pressure reaches the equilibrium vapour pressure. He proposes a theory, and develops formulae for the rate of bubble formation using the classical nucleation theory of Frenkel [**30**] and Volmer [**31**]. The fluid 'fracture pressure' is

the negative pressure p_{fract} at which the fluid 'fractures' and causes the appearance of the first gas bubble(s)

$$p_{\text{fract}} = -\left[\frac{16\pi}{3}\left(\frac{\sigma^3}{kT\ln(NkTt/h) - \Delta f_0}\right)\right]^{0.5}$$

where k is the Boltzman constant, N is the number of molecules, t is the time for the first bubble apparition, σ is the interfacial surface tension, and Δf is the free energy of activation. Fisher also tabulates (Table 1, [**29**]) the values of the waiting time t to the apparition of the first bubble for different free energy of activation for water. He also tabulates, for the same temperature ($T = 300\,^{\circ}\text{K}$), the 'fracture pressure' for different liquids when $\Delta f_0 = 0$ (Table 2, [**29**]). The calculated 'fracture pressure' for water is 132 MPa. This is approximately one order of magnitude higher than the maximum experimental value obtained for pure water on a regular surface, and two orders of magnitude higher for gassed water on irregular surfaces [**27**, **28**]. Hendricks *et al.* [**32**] present an analogy between cavitation and fracture mechanics, asserting that the role impurities play in the formation and propagation of a crack in solids parallels the role played by the first bubble of the fractured fluid [**29**] in the growth of the cavitation zone. Further, they analyse the similarities between the Griffith [**33**] and Fisher–Frenkel [**29**, **30**] crack models for solids and liquids, respectively. It is concluded that both models predict fracture-starting stresses that are significantly higher (10^2 orders of magnitude) than the ones yielded by experiments. As a result, a 'rule-of-thumb' is proposed, whereby all the theoretically obtained values are scaled ($p_{\text{fract}}/10^2$) in order to be brought in line with the experiments. The authors [**32**], further remark that photographs of crack propagation in solids and cavitation in bearings possess common features in that the main line crack and the attached secondary cracks have similar physical and propagation characteristics. Hoffman and Myers [**34**] also looked at cavitation, but in the context of the splitting of thin coating fluid films. Their intended application pertains to the roll application of these films. The authors use a heuristic approach by combining high-speed film analysis of the roll coating and film splitting with a partly theoretical approach. In the end, they present an equation that calculates the 'fracture pressure' at which the thin rolling film cavitates, ($\Delta P = [2(\sigma + 2\mu\text{V})/R] + 1.5\rho V^2$). The equation relates the pressure differential (ΔP) across the cavity to its growth velocity V by taking into consideration the interface (radius R), the inertial term (ρV^2), the surface tension term (σ), and the viscous term (μV).

The differentiating factor between a fluid and a solid state resides with the respective molecular cohesion forces which are dependent on the average intermolecular distances; these forces vary inversely proportional with the square of the aforementioned distance. When compared to those in the solid, the forces in the fluid are much smaller, and hence normal (tensile) stresses cannot be readily sustained. That is not to say that a liquid cannot sustain any tensile stresses [**3**, **4**]. Floberg [**35**] starting from a fixed mass gas bubble in an equilibrium-state condition in a fluid ($R^3\rho = R_0^3\rho_0$), determined that for adiabatic conditions the fluid pressure p is related to the bubble starting equilibrium pressure q_0 and surface tension T by

$$p = q_0 = \left[\frac{R_0}{R}\right]^{3k} - \frac{2T}{R}, \quad \text{where } \frac{q_0}{\rho_0^k} = \frac{q}{\rho_k}$$

while for isothermal conditions

$$p = q_0 = \left[\frac{R_0}{R}\right]^{3} - \frac{2T}{R}, \quad \text{where } \frac{q_0}{\rho_0} = \frac{q}{\rho}$$

where k is the adiabatic coefficient, R_0 is the starting bubble radius, and ρ is the density of the gas. The above equations reveal that as the fluid pressure, p, decreases, the bubble radius R, grows simply by pure expansion. This process, termed pseudo-cavitation, occurs with no additional gas diffusing into the bubble ($R_0^3\rho_0 = R^3\rho$). One could liken the pseudo-cavitation process to a balloon of fixed internal mass that starts expanding as the environmental pressure decreases. However, as the fluid pressure falls below the dissolved gas saturation pressure, the bubble increases in size due to additional mass input. This is a desorption process, a phenomenon during which non-condensable gases diffuse from the liquid phase into the existing gaseous bubble nucleus. As such, the bubble serves as a nucleus for fluid rupture with the ensuing 'crack' fueling the cavitation growth. For a homogeneous mixture of non-condensable gases, the relation $p < p_{\text{sat}}(T)$ has to be replaced by $p < p_{\text{gas sat},i}(T)$ (Fig. 1(b)). Due to diffusion, indicative of a lower tensile liquid strength, the bubble starts growing rapidly and exhibits rarely an unstable behaviour. This phenomenon is known as gaseous cavitation. The concepts presented above for pseudo- and gaseous cavitation address the issue of a gas bubble growth. More generally, this growth can occur due to either the lowering of pressure in the fluid without additional gas diffusion, or when the fluid pressure has crossed the threshold of the gas saturation pressure. The latter situation is characterized by a very rapid bubble growth.

For applications to bearings, the absorption and desorption of a non-reacting, non-condensable gas mixture has to be considered. The mixture total pressure can be determined by Dalton's law of additive pressures

$$P_{\text{mix}} = \sum_{i=1}^{n} p_{\text{gas sat},i}(T_{\text{mix}}, \forall_{\text{mix}})$$

where $p_{\text{gas sat},i}$ is the partial pressure of a component in the mixture that represents the individual gas (i)

Table 1 Pressures and temperatures for the release of gas and vapour for an 'example oil'

Nitrogen gas dissolved in oil						Example oil mixture components	
Temperature	Nitrogen saturation pressure, $p_{\text{gas sat},i}(T)$	Mole fraction, $y_{i,\text{liq side}}$	Volume fraction $V_{\text{gas}}/V_{\text{total}}$ (%)			Hydrocarbon component	Vapour pressure, p_{Vap}
(1)	(2)	(3)	(4)			(5)	(6)
150°C	344.8 kPa	0.006 41	0			$C_{10}H_{22}$ (n-decane)	52.4 kPa
	101.37(1 atm)	0.001 88	0.37	0		$C_{20}H_{42}$ (n-icosane)	0.14 kPa
	68.96	0.001 28	0.53	0.12	0	$C_{28}H_{58}$ (octa-cosane)	1.59 Pa
	34.48	0.000 64	0.82	0.50	0.34		
100°C	344.8 kPa	0.005 58	0			$C_{10}H_{22}$	9.5 kPa
	101.37	0.001 64	0.27	0		$C_{20}H_{42}$	5.1 Pa
	68.96	0.001 12	0.38	0.058	0	$C_{28}H_{58}$	0.015 Pa
	34.48	0.000 56	0.62	0.263	0.155		
65°C	344.8 kPa	0.005 12	0			$C_{10}H_{22}$	1.9 kPa
	101.37	0.001 51	0.24	0		$C_{20}H_{42}$	0.21 Pa
	68.96	0.001 02	0.35	0.055	0	$C_{28}H_{58}$	2.1E-4 Pa
	34.48	0.000 51	0.54	0.203	0.116		

saturation pressures in the liquid. The corresponding law of volumes is given by Amagat's law

$$\forall_{\text{mix}} = \sum_{i=1}^{n} \forall_{\text{gas sat},i}(T_{\text{mix}}, P_{\text{mix}})$$

Defining the mole fraction of the ith component as $y_{i,\text{gas side}} = N_{\text{i}}/N_{\text{mix}} = p_{\text{gas sat},i}/P_{\text{mix}}$, the individual gas saturation pressures can be written in terms of the total mixture pressure, P_{mix}, as

$$p_{\text{gas sat},i} = y_{i,\text{gas side}} P_{\text{mix}}$$

Most gases are weakly soluble in liquids. It has been found that for such situations the relationship between the mole fraction of the ith species in the gas mixture and in the liquid, at their interface, is governed by $y_{i,\text{gas side}} \propto y_{i,\text{liq. side}}$. Then, based on Dalton's law and the mole fraction definition one can write $p_{\text{gas sat},i} \propto y_{i,\text{liq. side}} P_{\text{mix}}$. This is known as Henry's law where the proportional sign can be eliminated if one introduces Henry's constant $H(= P_{\text{mix}}$ *prop.const.). Then

$$y_{i,\text{liq. side}} = \frac{p_{\text{gas sat},i}}{H}$$

The concentration of an ith species dissolved in the liquid is proportional to the partial pressure of the gas, and is inversely proportional to Henry's constant. It has been noted that H increases with increasing temperature. The above observation, in combination with the bearing's divergent zone heat dissipation and decreasing pressure, is responsible for the significant decrease in $y_{i,\text{liq. side}}$. This lower $y_{i,\text{liq. side}}$ is indicative of the gas being released from the oil and migrating into the existing bubble, thus exacerbating its accelerated and extensive growth. For the case when the gas is strongly soluble in the fluid, Henry's law gives way to Raoult law

$$y_{i,\text{liq. side}} = \frac{y_{i,\text{gas side}} P_{gas,\,total}}{p_{\text{gas sat},i}(T)}$$

where, by Dalton law

$$P_{\text{gas,total}} = \sum_{i=1}^{n} p_{\text{gas sat},i}(T)$$

The above equations, taken in conjunction with Floberg's adiabatic or isothermal bubble's pressure equations may be used to explain the non-condensable gas mixture bubble formation and growth in a bearing environment. Normally, mineral oils contain some amounts of dissolved gas at pressures near the atmospheric pressure. As the pressure in the bearing falls below the $p_{\text{gas sat},i}$ of the individual ith gas component, the latter is released from the oil and diffuses into the gaseous bubble. For this purpose, let the 'example oil' presented in Table 1 be examined. The oil is a mixture of hydrocarbon fractions of n-decane, n-icosane, and octa-cosane. The table gives the following:

(a) the vapour pressures, p_{Vap}(T), for each respective component;
(b) an estimate of the nitrogen gas saturation pressures, $p_{\text{gas sat},i}(T)$;
(c) the mole and volume fractions of nitrogen dissolved in this oil.

Column (4) shows the volume fraction of nitrogen dissolved in this hydrocarbon mixture at the given temperatures and the nitrogen saturation pressures shown in column (2). For example, consider a nitrogen mole fraction (column (3)) of $y_{i,\text{liq side}} = 0.006\,41$ at 150 °C and 344.8 kPa. If the pressure drops isothermally to 101.37 kPa (atmospheric), the mole fraction

on the liquid side becomes $y_{i,\text{liq side}} = 0.001\,88$. This means that 0.004 53 of the dissolved gas has diffused into the gas side bubble. In terms of volume fraction (column (4)), the volume the gas now occupies represents 37 per cent of the total volume. If pressure is dropped further to 34.48 kPa the volume fraction of gas grows to 82 per cent, even though the mole fraction on the liquid side has decreased only by a $\Delta y_{i,\text{liqside}} = 0.001\,24$. This means that 82 per cent of the total volume is now occupied by the nitrogen. From columns (5) and (6), respectively, it can be seen that only when the pressure is dropped to 52.4 kPa, at 150 °C, does n-decane come out of the oil in the form of vapour. Assuming the process is isothermal, it means that until pressure reaches the threshold of 52.4 kPa, only gaseous cavitation takes place. At 52.4 kPa the first vapour traces of n-decane appear, and beyond this pressure threshold there will be a combination of gaseous and vaporous content in the bubble. As operating temperatures are decreased to 100 °C and then 65 °C the threshold at which the first n-decane vapour is generated is lowered dramatically to 9.5 and 1.5 kPa, respectively. For the other components of this oil the vapour pressure is even lower, precluding any generation of n-icosane or octa-cosane vapour. All the while, the volume fraction of nitrogen grows considerably to maxima of 62 per cent and 54 per cent as $p_{\text{gas sat},i}(T)$ decreases.

The section above describes the formation and growth of 'gaseous cavitation', while Table 1 exemplifies indeed the very low pressure conditions necessary to release hydrocarbon vapour.

Cavitation can 'fracture' the fluid through a phase change. This phenomenon is known as 'vaporous cavitation'. 'Gaseous cavitation' forms and grows as the pressure in the liquid falls below the saturation pressure, $p_{\text{gas sat},i}$ (Fig. 1(b)). 'Vaporous cavitation' occurs when the pressure in the fluid falls below the vapour pressure of the liquid, $p_{\text{Vap}} = p_{\text{sat}}$ (Fig. 1(b)). 'Vaporous cavitation' is very different from the 'gaseous' one, both through the composition of the gases that fill the cavity and the thermodynamic environment that causes its occurrence. To explain this form of cavitation, one has to start from the kinetic theory of liquids. In his now famous treatise on kinetic theory of liquids, Frenkel [**30**] states:

> The fact that the liquids can withstand or exert a negative pressure is implied by the van der Waals theory which is based on the assumption of a close similarity between the liquid and the gaseous state…according to this theory both states represent two extreme forms of a single amorphous state, one of which can be obtained from the other by isothermal compression or expansion…

This change in pressure is continuous and leads to a transitory state which is metastable in nature. The pressure volume (PV) diagram of Fig. 2 presents

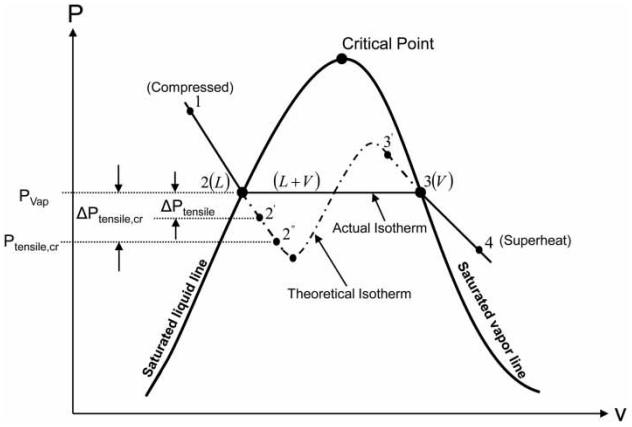

Fig. 2 The PV diagram for a hypothetical lubricating fluid

just such a situation. Again, according to Frenkel, the transition from the liquid state to vapour…

> '…takes place not along the theoretical isotherm (full line), but along of a horizontal isotherm corresponding to the splitting of the original homogeneous substance into two different coexisting phases…'

Of course, these two coexisting phases are the liquid and its respective vapour phase. If state (1) is identified as a pure liquid compressed along the isotherm T, and then the fluid is depressurized along the same isotherm to the point of the saturated vapour pressure represented by state $(2(L))$, two coexisting phases appear. These two phases are the saturated liquid and vapour $(L + V)$. These are components of the *'single amorphous state'* mentioned by Frenkel. According to him, the state of this mixture moves horizontally, under constant pressure, along the real isotherm, to state $(3(V))$. At this juncture, the fluid becomes all vapour, and if the pressure were to fall further, the fluid may find an equilibrium state as indicated by the superheated vapour state (4). This path is followed if during the depressurization sequence there were 'enough' pre-existing nucleation sites. They may be provided by the gas trapped in the crevices at the solid/fluid interface, or outright in the bulk mass of the liquid. They serve the same role in the cracking/splitting of the fluid as the impurities would play in the crack propagation in a solid, Hendricks *et al.* [**32**]. According to Brennen [**36**], if nucleation sites are not present, whether due to degassing, or the smoothness of the mating surfaces, the state reached at point $(2, (L))$ continues along the theoretical isotherm to $(2')$, rather than moving horizontally along the real isotherm towards $(3,(V))$. Note that on the actual isotherm $p_{2(L)} = p_{\text{Vap}} = p_{3(V)}$. The pressure at point $2'$ is lower than at $(2(L))$, and the liquid is said to be in tension, at a value of $\Delta p_{\text{tensile}} = p_{2'} - p_{\text{Vap}} < 0$. The liquid is said to be now in a metastable state, a state of instability which may cause an abrupt transition from $(2')$

to (4). This abruptness may create an instantaneous cavitation zone, vaporous in nature. For a pure substance, the vapour cavity contains the same species as the liquid zone. In the case of homogeneous mixtures, as many of the mineral oils are, each of the fractional components of the oil has its own 'vapour pressure', and starts to evaporate as its particular p_{Vap} is reached. For further insights into the tensile strength of fluids and nucleation theory the reader is referred again to Frenkel [**30**] and Brennen [**36**]. It is to be noted that cavitation and boiling manifest in same way, their end-effect being the generation of vaporous zones. However, the thermodynamic drivers that lead to the vaporous state are different. Vaporous cavitation occurs when the build-up of tensile stresses in the form of $(p_{2'} - p_{\text{Vap}})$ reaches or exceeds the critical value, $\Delta p_{\text{tensile,cr}} = (p_{2'} - p_{\text{Vap}}) \ll 0$. In vaporous cavitation, the vapour pressure is determined by following a constant isotherm. Boiling, however, occurs when the rising fluid temperature reaches or exceeds the critical saturation temperature, T_{sat}. In boiling, the saturation temperature is determined by following a constant isobar. If the amount of superheat responsible for boiling is measured, the Clausius–Clapeyton equation can be used to write a relationship correlating the critical tensile pressure and critical temperature as

$$\Delta p_{\text{tensile, cr}} \approx \Delta T_{\text{cr}} \frac{h_{\text{fg}} \rho_V}{T} \text{ (for } \rho_L \gg \rho_V)$$

Even though the above equation is valid only for small amounts of excess superheat, it establishes a valuable connection between $\Delta p_{\text{tensile,cr}}$ and ΔT_{cr}. Vaporous cavitation may thus appear either due to the following:

(a) excess tensile stresses beyond the critical point;
(b) increases in temperatures beyond the critical amount of superheat, or more generally;
(c) be a combination of these two.

The 'cavitation number' below correlates the above concepts and is used as an indicator for the prediction of vaporous cavitation

$$\sigma = \frac{p_\infty - p_{\text{Vap}}(T_\infty)}{0.5 \rho_L U_\infty^2}$$

In this equation, p_∞ and T_∞ represent the bulk fluid pressure at the corresponding temperature. For a bearing, U_∞ is the rotor surface velocity, and p_{Vap} is the vapour pressure at the corresponding temperature T_∞. Parametrically, the cavitation number can be used to study and classify the inception of cavitation in flows where either p_∞ is decreased to values equal or smaller than $p_{\text{Vap}}(T_\infty)$, or the free stream velocity U_∞ is increased causing a significant decrease in σ. As σ decreases it approached the threshold point σ_{cr}, which defines the incipient formation of vaporous cavitation. Thus, predictions of cavitation incipience and subsistence can be drawn from calculations, measurements, and observations of σ_{cr} in conjunction with the Clausius–Clapeyron relationship and data relating to the theoretical isotherms.

3 FILM RUPTURE THEORETICAL MODELLING

3.1 The Gumbel and Swift-Stieber Models

Cavitation bubbles whether gaseous or vaporous may come from within the lubricating film, or be fed by the environment. Regardless, they represent a rupture in the continuity of the liquid film. This discontinuity at the bubble interface presents a challenge in the context of the solution to the Reynolds equation. The solution offered by Sommerfeld [**2**], did not take into account film rupture and solved for a full film around the circumference (Figs 1(a) and (b)). This approach allowed subatmospheric and even negative pressures, no matter how low they were [**16**]. Gumbel [**37**] in 1914 was the first to account for the film 'rupture'. According to his theory, for a steadily loaded bearing operating at constant angular velocity, the rupture originates in the immediate vicinity of the film's minimum clearance, at a predetermined pressure p_{cav} and remains constant at that value for the entire divergent region (Fig. 3(a)).

He did not account for film reformation, nor did his approach respect mass continuity. Because the circumferential pressure distribution allows only the positive pressure region, the Gumbel condition is also known as the 'half-Sommerfeld' condition (Fig. 3(a)). It represents an early simplistic approach that recognizes the observed physical reality of the film rupture and embodies it into an analytical and numerical simulation. A better alternative to the 'half-Sommerfeld' condition was offered by Swift [**38**] and Stieber [**39**], which worked independently of each other (Fig. 3(b)). Swift [**38**] in 1932 stated that a zero derivative of the pressure is an appropriate condition for marking the inception of cavitation and considered it to be a 'stability condition'. Stieber [**39**] in 1933 published a full solution for a 360 deg journal bearing considering cavitation for a zero tensile strength lubricant (Floberg later offered different approaches for the zero and non-zero tensile stress in lubricant's cavitation [**40**]). Stieber, like Swift, assumed a zero-pressure gradient at the start of the cavitation zone, but considered it to be a continuity condition. These two forefathers of cavitation modelling, while approaching it from different angles, came to the same conclusion regarding its inception and development. The cavitation zone formation conditions known as the Swift–Stieber conditions (Fig. 3(b)) are

$$\frac{\partial p}{\partial x} = \frac{\partial p}{\partial y} = 0, \quad p = p_{\text{cav}}$$

Note that these conditions consider the entire cavitation zone at $p = p_{\text{cav}}$ and do not make allowance

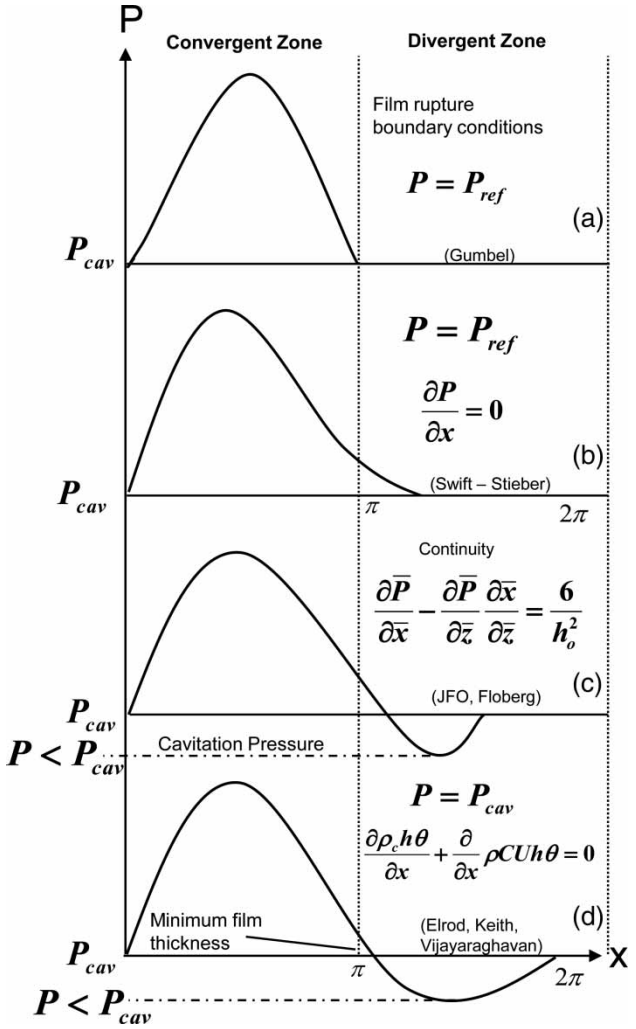

Fig. 3 Circumferential pressure development based on film rupture theories: (a) Gumbel [**37**]; (b) Swift–Stieber [**38**, **39**]; (c) JFO and Floberg; and (d) Elrod [**53**], and Vijayaraghavan and Keith [**54**, **55**]

for the existence of subcavitational pressures nor for variations in the pressure inside the cavitation zone. After film rupture the Poiseuille (pressure driven) component of the circumferential and axial velocities becomes zero, and only the Couette (shaft rotation, or axial oscillation) component is still operational, carrying lubricant in between the gas cavities (Fig. 4(a)). A constant cavity pressure imposes a zero-pressure gradient within the cavity. The pressure gradient calculated in the fluid has to interface with the cavity pressure gradient along the boundary, where at certain locations there can be a relatively steep slope (e.g. the point of cavity inception). According to Floberg [**40**], these boundary conditions work well at moderate loads. According to Brewe *et al.* [**14**], while the Swift–Stieber conditions work reasonably well for the establishment of the film rupture, they do not predict the reformation of the film satisfactorily; nor do they seem to give satisfactory results in the case of dynamically loaded bearings [**14**, **41**].

3.2 Flow separation boundary conditions

Floberg [**40**, **42**, **43**] experimentally showed that subcavity (subambient) pressures do occur in bearings. Their existence led to the belief that flow separation takes place and contributes to the film rupture. In 1968, Mori *et al.* [**44**] offered a set of conditions predicting film rupture and cavitation inception. They considered that when separation takes place, it starts at the stationary surface of the bearing when $\mathrm{d}u/\mathrm{d}y|_{y=0} = 0$ and $p = p_{\mathrm{cav}}$ (Fig. 4(b)). These conditions are present at the free surface between the liquid and the cavitation bubble. This approach to cavitation modelling has given acceptable results, but only for a limited number of cases [**40**]. Based on the experimental observation of subcavity pressures Hopkins [**45**] in 1957, and then Birkhoff and Hays [**46**] in 1963 also pointed to flow separation as a possible reason for film rupture. They applied their analysis to a full fluid film, and employed the same boundary conditions (as in [**44**]) at the stationary surface ($u = \mathrm{d}u/\mathrm{d}y|_{y=0} = 0$) (Fig. 4(b)). Then, using the Navier–Stokes equations (NSE), where the advective terms are neglected, and solving with the above boundary conditions for the u-velocity, one obtains

$$u = \frac{1}{2\mu}\frac{\partial p}{\partial x}(y^2 - h^2) + U$$

From this expression, considering that at the point of cavity inception ($y = 0$) the velocity is zero ($u(y = 0) = 0$), the resultant pressure-gradient condition can be written as

$$\left.\frac{\partial p}{\partial x}\right|_{y=0} = \frac{2\mu U}{h^2}$$

With the cavitation pressure set at $p = p_{\mathrm{cav}}$, and velocity and pressure gradients for film rupture conditions known, one can start calculating the approximate position of the cavitation region.

Under this scenario, the majority of the lubricant will be carried either under or above the cavitated region (Fig. 4(b)), and not in-between the gas fingers as implied by the Swift–Stieber condition (Fig. 4(a)). Coyne and Elrod [**47**] introduced the effects of geometry, surface tension, and inertia in modelling the phenomenon of planar film rupture (no side leakage) (Fig. 4(c)). They proposed a modified form of the pressure gradient when compared to the one put forward by Birkhoff and Hays [**46**] and Hopkins [**45**]. By preserving mass continuity at the gas/liquid interface they

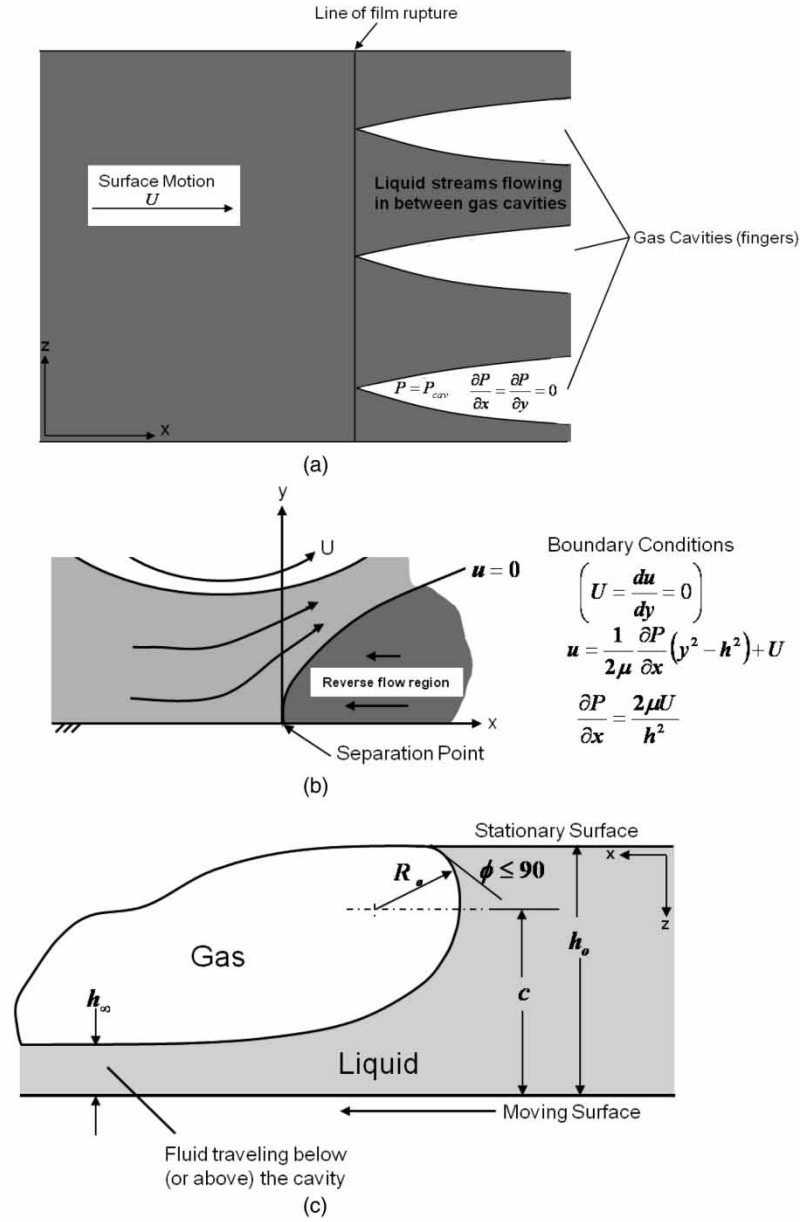

Fig. 4 Film rupture boundary conditions types: (a) striated gas and liquid fingers (Swift Stieber, JFO); (b) Hopkins and Birkhoff [**11**, **46**] separation boundary conditions (full fluid film); and (c) Coyne and Elrod [**47**, **48**] boundary conditions (gas–fluid interface)

obtained

$$\frac{\partial p}{\partial x} = \frac{6\mu U}{h^2}\left(1 - 2\frac{h_\infty}{h}\right)$$

$$\text{where} \quad \frac{h_\infty}{h} = \frac{c}{h_\infty}\left(1 + \frac{R_0}{c}\cos\varphi\right)$$

The angle φ represents the stationary surface wetting angle and is $\varphi \leqslant \pi/2$. The terms c/h_∞ and R_0/c are both functions of a surface-tension parameter $N = \sqrt[3]{(3\mu U/T)}$ and are calculated in reference [**47**]. In addition to the pressure gradient boundary condition, Coyne and Elrod [**48**] introduced a pressure boundary condition of the form

$$p = \frac{-T}{R_0} + \Delta p$$

where T is the surface tension at the gas liquid/gas interface, and R_0 is the radius of curvature of the bubble (Fig. 4(c)). The film pressure near the stationary surface boundary is $-T/R_0$, while Δp represents a transition pressure correction that is small in comparison to the surface-tension term when N is small. These two boundary conditions lead to the determination of the liquid/gas interface position and the local accompanying pressure.

3.3 The mass conservation model

The more elusive problem in dealing with film rupture has been respecting mass continuity within the confines of the Reynolds equation. Gumbel's condition [**37**] did not respect the continuity of mass; it just accounted for the fact that when and where the film ruptured pressures became subambient (negative) and consequently automatically set to p_{cav}. The more advanced Swift–Stieber model [**38**, **39**] accounts for the entire mass of liquid transported in-between (Fig. 4(a)) the gas fingers (cavities), but does not take into account the fingers' number, size, and volume. This approach sets the pressure gradients to zero, and as the pressure increases in the convergent region allows the film reformation process to take place. Unlike Swift–Stieber, the separation models of Coyne and Elrod [**47**, **48**], Mori *et al.* [**44**], Hopkins [**45**], and Birkhoff and Hays [**46**] provide for the fluid transport above and beneath the bubble. All these models use continuity of mass to define the cavity interface. However, notwithstanding their success, none of them were able to handle well the situation of a moving liquid/gas boundary where mass was conserved both in the cavitated region as well as on the boundary. Floberg [**40**], Jakobson and Floberg [**49**], Olsson [**50**], and Floberg [**51**] again assumed, similarly to Swift and Stieber, a striated flow (Fig. 4(a)), where the liquid was transported in-between gas fingers that extended fully across the clearance between the stationary and the moving surfaces. These contributions, made by the respective authors independent of each other, are referred to as the Jakobson, Floberg and Olsson (JFO) cavitation theory [**14**, **52**]. Conserving mass across the entire bearing based on the Reynolds equation model has proven seminal to the most recent advances in the numerical implementation of cavitation. Floberg [**40**, **51**] differentiated his analysis for two cases of liquid lubricant tensile strength.

3.3.1 The case of liquid with zero tensile strength

Generally, oils have low tensile strength which may decrease even more if large amounts of gas are dissolved in the oil. Film rupture occurs when the respective gas saturation pressure is reached; the latter becomes the bearing cavitation pressure and this pressure remains constant throughout the cavitated (striated) zone. The gas and oil coexist in an alternate pattern of oil regions and gas fingers; as a result, only a Couette-type flow is active in transporting the liquid in-between the gas fingers. Figure 5 presents the influx and efflux of mass across the bubble control surface. This surface defines the gas striation control volume.

In this two-dimensional space the continuity equations at the upstream (1) and downstream (2) locations of the boundary can be written as

$$\dot{m}_{x,i}\mathrm{d}z - \dot{m}_{z,i}\mathrm{d}x = \dot{m}_{\text{cav}}\mathrm{d}z, \quad \text{where } i = 1, 2$$

Neglecting the inertia terms, and considering constant properties the simplified form of the NSE yield expressions for velocities u and w in the x- and z-directions, respectively. Upon the integration of these velocities across the fluid film between the moving and stationary members one obtains the following flows

$$\dot{m}_{x1} = \frac{Uh_1}{2} - \frac{h_1^3}{12\mu}\left(\frac{\partial p}{\partial x}\right)_1$$

$$\dot{m}_{z1} = \frac{h_1^3}{12\mu}\left(\frac{\partial p}{\partial z}\right)_1$$

$$\dot{m}_{\text{cav}} = \frac{Uh_1}{2}$$

Introduction of the above mass flowrate expressions into the continuity equation on the bubble boundary at location (1) results in the following condition

$$-\frac{h_1^3}{12\mu}\left(\frac{\partial p}{\partial x}\right)_1 + \frac{h_1^3}{12\mu}\left(\frac{\partial p}{\partial z}\right)_1\left(\frac{\mathrm{d}x}{\mathrm{d}z}\right)_1 = 0$$

Since no tensile stresses (negative pressures) are permitted in the film, to satisfy the bubble boundary continuity equation it is necessary that $\partial p/\partial x|_1 = \partial p/\partial z|_1 = 0$. These now become the boundary conditions for the inception of the cavitation bubble. Additionally, one has to specify the cavitation pressure p_{cav} which remains constant throughout the cavitation region. Following the same procedure for control volume (2) (Fig. 5(a)), one can write

$$\dot{m}_{x2} = \frac{Uh_2}{2} - \frac{h_2^3}{12\mu}\left(\frac{\partial p}{\partial x}\right)_2$$

$$\dot{m}_{z2} = \frac{h_2^3}{12\mu}\left(\frac{\partial p}{\partial z}\right)_{12}$$

$$\dot{m}_{\text{cav}} = \frac{Uh_1}{2}$$

Further, applying the continuity equation for control volume (2) one obtains a mass conservation condition for the bubble downstream reformation boundary

$$-\frac{h_2^3}{12\mu}\left(\frac{\partial p}{\partial x}\right)_2 + \frac{h_2^3}{12\mu}\left(\frac{\partial p}{\partial z}\right)_2\left(\frac{\mathrm{d}x}{\mathrm{d}z}\right)_2 + \frac{Uh_2}{2} = \frac{Uh_1}{2}$$

Solving the Reynolds equation in conjunction with the above-mentioned boundary conditions for film rupture and reformation ones obtains a set of pressure contour profiles like the one shown in Fig. 6 (see also reference [**40**]).

The positive pressure contours are in the region of the applied load while the theoretical cavitation zone is marked by the subcavity pressure contour lines.

3.3.2 The case of liquid with finite tensile strength

Based on experimental results, Floberg further postulated [**40**, **51**] that when the fluid can sustain a certain

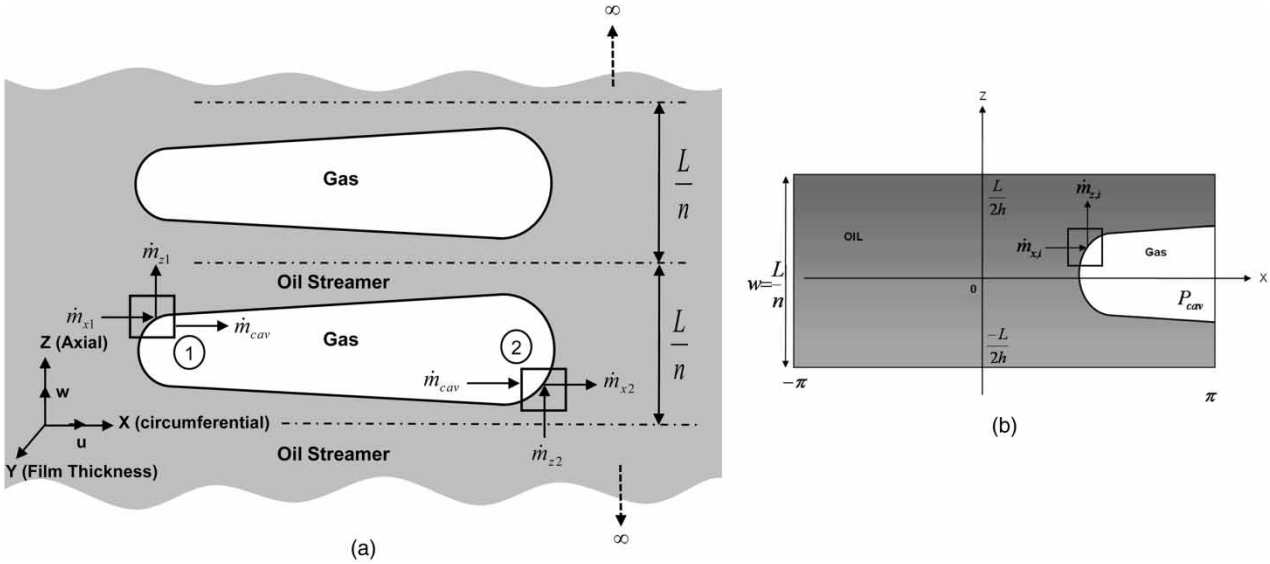

Fig. 5 (a) Geometry of the oil cavity used in the JFO type theory. Typical cavitation bubbles for a zero tensile strength liquid with mass continuity control volumes at the upstream inception (1) and downstream reformation (2) and (b) Geometry is for one repetitive cell for a liquid with finite tensile strength for a finite (or infinite numbers of such cells) with the width of the cell $W = L/n$

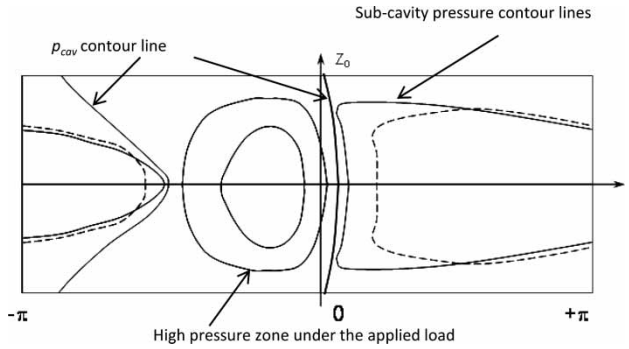

Fig. 6 Pressure contour lines in a journal bearing using the JFO theory for a liquid with zero tensile strength; one gas bubble, one oil streamer occupying the width of the bearing

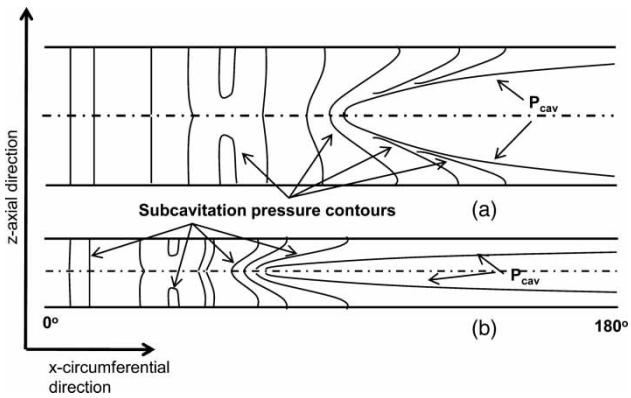

Fig. 7 Pressure profiles in a journal bearing using the JFO theory for a liquid with tensile strength, as a function of the number n of oil streamers

tensile strength, a finite number of liquid streams will form and flow in-between the gas cavities, with negligible quantities of oil entering or exiting the gas streamers ($\dot{m}_{\text{cav}} = 0$, Fig. 5(b)). The cavitation pressure is no longer the lowest pressure in the bearing, since the dissolved gas saturation pressure is different from, and in most cases higher than the tensile stress that the fluid is subject to in the divergent zone (Fig. 3(c)). While the gas saturation pressure remains constant, the drop in pressure ('negative pressure') is a strong function of the journal rotation.

In an infinitely long bearing, a repetitive number of 'oil stream/gas fingers' cells form covering the entire axial bearing width. This makes it sufficient to calculate just one characteristic cell. Then, one can identify a characteristic width per oil stream ($W = L/n$), where the number of oil streams, n, is related to the tensile strength of the fluid [**40**]. Thus, the parameter n becomes part of the analysis, which can now be confined to a single cell of width W. Using the geometry presented in Fig. 5(b), and noting that in this case $\dot{m}_{\text{cav}} = 0$, for the single cell, one can perform the same type of analysis as for a zero tensile strength lubricant. Then, the continuity equation for the control volumes ($i = 1, 2$) (Fig. 5(b)) becomes

$$\dot{m}_{x,i}\mathrm{d}z - \dot{m}_{z,i}\mathrm{d}x = 0$$

The upstream boundary condition becomes

$$-\frac{h_2^3}{12\mu}\left(\frac{\partial p}{\partial x}\right)_2 + \frac{h_2^3}{12\mu}\left(\frac{\partial p}{\partial z}\right)_2\left(\frac{\mathrm{d}x}{\mathrm{d}z}\right)_2 = -\frac{Uh_1}{2}$$

while the downstream (or reformation) one becomes

$$-\frac{h_2^3}{12\mu}\left(\frac{\partial p}{\partial x}\right)_2+\frac{h_2^3}{12\mu}\left(\frac{\partial p}{\partial z}\right)_2\left(\frac{\mathrm{d}x}{\mathrm{d}z}\right)_2=-\frac{Uh_2}{2}$$

Floberg solved the Reynolds equation in conjunction with the above boundary conditions for the film rupture and reformation. A typical qualitative result depicting the formation of the cavitation region is shown in Fig. 7 (see also reference [**51**]). Note that the associated subcavitation pressure contours are a function of the n number of streamers. For the interested reader, Floberg [**51**] presents a detailed dimensionless model implementing cavitation for the infinitely long bearing. The parametric study discusses the quantitative pressure contours for one oil stream/cavity at different values of the parameter n (Fig. 6 of reference [**40**] and Figs 8 to 11 of reference [**51**]). For finite width bearings, the solution is more intricate [**49**] because each 'oil stream/gas finger' cell has to be evaluated separately and the numbers of cells formed has to be simultaneously calculated. The solution strictly satisfies flow continuity in all bearing regions. The authors apply it to bearings without oil grooves, and account fully for the vaporous/gaseous cavitated regions. They emphasize that the choice of 'arbitrary' rupture and reformation boundaries of the cavitated region yields only approximate pressure distributions, load-carrying capacities, and power losses. The method was also applied to optimize a bearing operating under cavitated conditions by calculating a minimal power loss for a given load, angular velocity, and permissible minimum film thickness. The experimental work presented in the same study [**49**], successfully validated the cavitation model.

3.3.3 *Other Reynolds equation-based cavitation computation models*

The concept introduced by the JFO theory has been widely accepted and adopted. Additionally, various numerical algorithms have been proposed for its implementation. In 1974, Elrod and Adams [**52**] obtained a generalized form of the Reynolds equation and solved it numerically making use of the JFO concept. They offered a substantially simpler way of accounting for mass conservation within the cavitated and non-cavitated regions. The authors introduced a new dimensionless density variable $\theta=\rho/\rho_c$, where the density ρ_c corresponded to the cavitation pressure p_{cav}. Introducing the notion of a bulk modulus (or the compressibility factor, $\beta=\rho\partial p/\partial\rho$) and integrating it for a constant β they obtained an expression that related the pressure p, to the cavity pressure (p_{cav}) and its dimensionless density θ, as $p=p_{cav}+\beta\ln\theta$.

Introducing the expressions for β and θ and a new switch function $g=g(\theta)$ into the standard Reynolds equation, they obtained a θ-modified form that was solved for θ

$$12\frac{\partial(\theta h)}{\partial t}+6U\nabla(\theta h)=\nabla\cdot\frac{h^3}{\mu}\beta g(\theta)\nabla\theta$$

This equation was solved numerically, by means of a finite-difference method, using mass conserving boundary conditions consistent with the JFO theory. This algorithm respects strictly mass continuity in all regions of the bearing, and most importantly uses one single equation for both the full film and the cavitated regions. This latter feature was achieved by the introduction of the switch function g, which functions as a 'cavitation index' in combination with the dimensionless density θ. By setting $g(\theta)=1$ when ($p\geqslant p_{cav}$ and $\rho\geqslant\rho_c$) and $g(\theta)=0$ when ($p\leqslant p_{cav}$ and $\rho\leqslant\rho_c$), the θ-modified Reynolds equation can be solved seamlessly for both the cavitated and non-cavitated regions. In the cavitated zone, the mass content of liquid is governed by ρ_{cav},θ, and h (as $\rho_{cav}\theta h$), where h is the eccentric clearance height. This means that θ, besides being a dimensionless density, also assumes the role of the fraction of liquid content in the cavity, with $(1-\theta)$ representing the cavity void fraction. After the θ solution is obtained, the pressure map can be reconstructed using $p=p_{cav}+\beta\ln\theta$. In 1981, Elrod further refined the methodology proposed in 1974 by presenting a computational algorithm [**53**], meant to be more user-friendly, even though the physics of the new model were the same as the ones presented earlier. The new version simplified the programming and made the complex task of cavitation modelling easier to handle. The results of the efforts undertaken by Elrod and Adams [**52**] and Elrod [**53**] produced an algorithm that is now universally accepted as 'the Elrod's cavitation algorithm'. Vijayaraghavan and Keith [**54**, **55**] used the JFO concept and modified the Elrod algorithm [**53**] to further refine the computational efficiency. They coupled directly the bulk modulus with the switch function and θ to obtain $g\beta=\theta(\partial p/\partial\theta)$. Upon integration of this equation one obtains an expression for pressure as

$$p=p_{cav}+g\beta\ln\theta$$

Then, by introducing the definition of θ and $g\beta$ into the standard Reynolds equation of the form

$$\frac{\partial\rho h}{\partial t}+\frac{\partial}{\partial x}\left(\frac{\rho hU}{2}-\frac{\rho h^3}{12\mu}\frac{\partial p}{\partial x}\right)+\frac{\partial}{\partial x}\left(-\frac{\rho h^3}{12\mu}\frac{\partial p}{\partial z}\right)=0$$

they obtained a Reynolds modified θ equation that can be solved for the entire bearing circumference

$$\frac{\partial\rho_c h\theta}{\partial t}+\frac{\partial}{\partial x}\left(\frac{\rho_c hU}{2}\theta-\frac{\rho_c h^3 g\beta}{12\mu}\frac{\partial\theta}{\partial x}\right)+\frac{\partial}{\partial x}\left(-\frac{\rho_c h^3 g\beta}{12\mu}\frac{\partial\theta}{\partial x}\right)=0$$

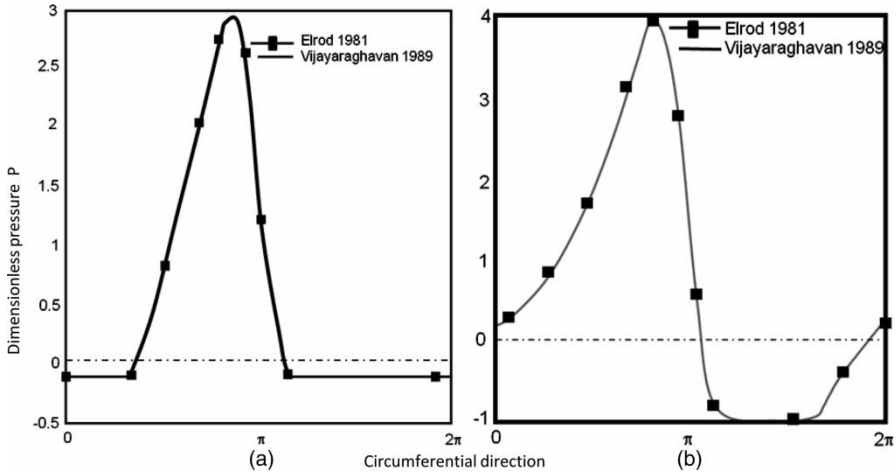

Fig. 8 Circumferential pressure profiles using the JFO concept through an improved algorithm Vijayaraghavan [**55**]: (a) high gas saturation pressure and (b) low gas saturation pressure

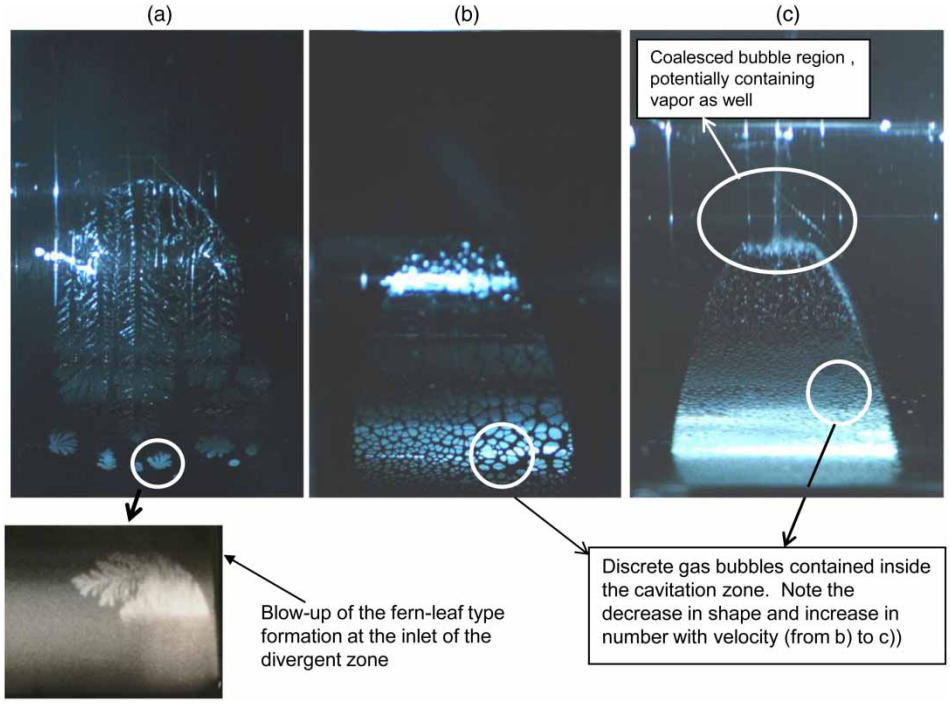

Fig. 9 Shape of the cavitation region in a two-phase damper at different speeds: (a) 700 r/min, incipient gaseous cavitated region with the fern-leaf formation clearly visible (see blow-up detail; (b) 1500 r/min, gaseous cavitated region showing the separated component bubbles; and (c) 3000 r/min, many of the gas bubbles coalesce in a larger formation

Then noting that in the cavitation zone, based on the assumption that the liquid is transported only through Couette effects (Swift–Stieber–Jakobson–Floberg–Olson assumption), and that $p = p_{\text{cav}}$, the equation above simplifies to

$$\frac{\partial \rho_c h\theta}{\partial t} + \frac{\partial}{\partial x}\left(\frac{\rho_c h U}{2}\theta\right) = 0$$

Figures 8(a) and 8(b) present examples of typical circumferential pressure profiles obtained by Vijayaraghavan and Keith [**55**]. In these figures, the constant cavity pressure is evident and the extent of the cavitation is clearly delineated. In Fig. 8(a), it can be seen that the cavitation pressure is just slightly below the atmospheric pressure, and the results are similar to those obtained by implementing the Swift–Stieber conditions.

In Fig. 8(b), the non-dimensional cavitation gauge pressure is much lower indicating a low gas saturation pressure $P = (p/\mu\omega)/(c/R)^2 = -1$. The results presented in Fig. 8 show very good agreement with those obtained by Elrod [**53**] and are also confirmed by the experimental results of Jakobson and Floberg [**49**].

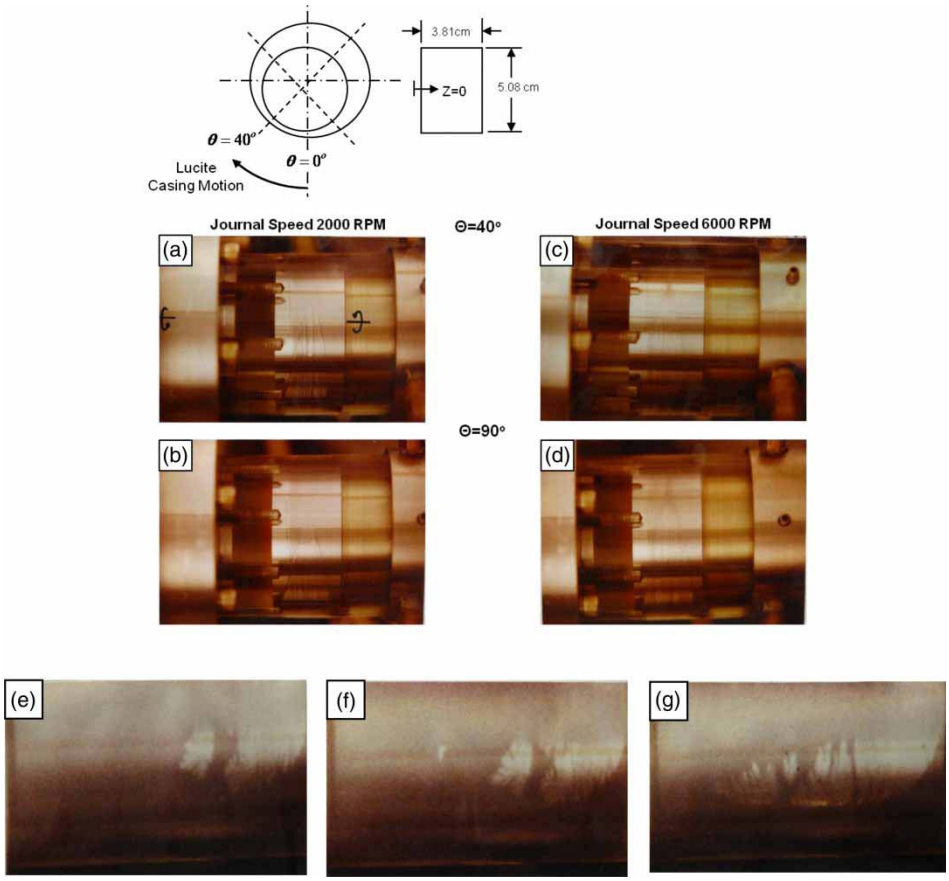

Fig. 10 Gaseous cavitation in a hydrodynamic submerged journal bearing (a)–(d) cavitation and reformation of the film at 2000 and 6000 r/min, respectively (e)–(g) fern-leaf patterns at the start of a cavitation process in the submerged journal bearing

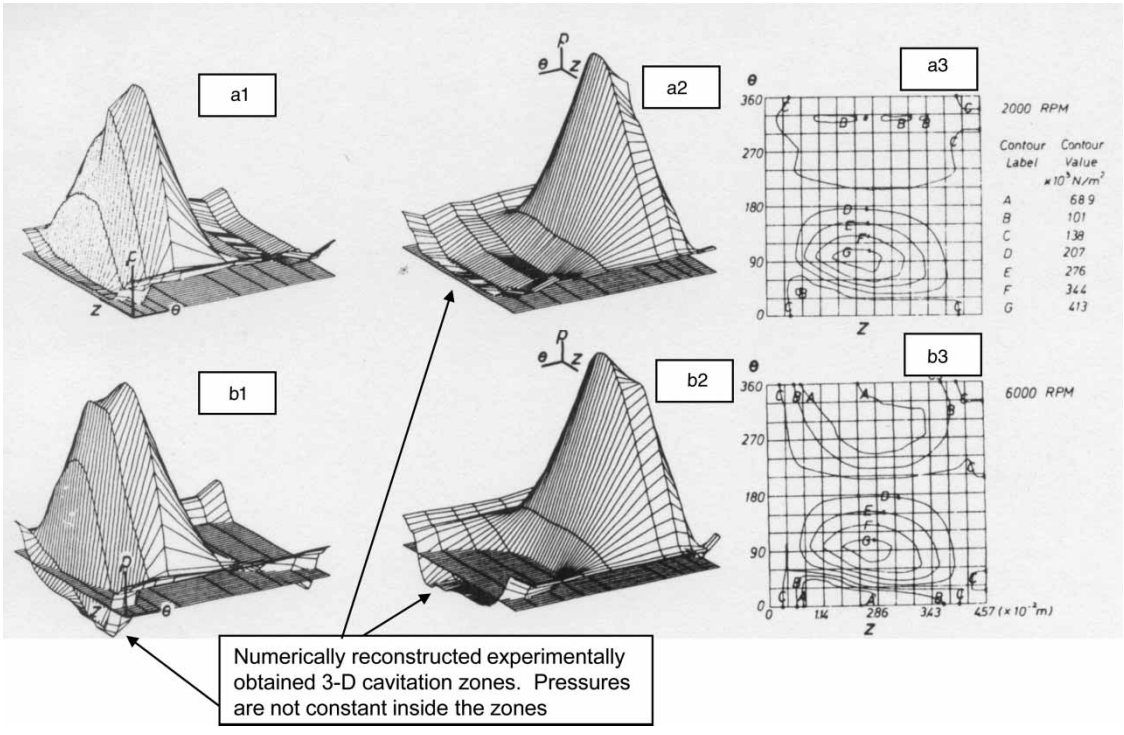

Fig. 11 Experimental pressure maps corresponding to the cavitation zones visualized in Figs 10(a) and (d), respectively

Vijayaraghavan and Keith further developed and tested their modified algorithm [**55**] on orthogonal and non-orthogonal grid arrays [**56**] as they were applied to finite grooved and misaligned grooved bearings [**57**].

Brewe [**41**] noted that while the present day bearings' high speed and loads combined with complex loading cycles may cause cavitation-induced erosion-like damage as described by Wilson [**25**], dynamic loading can also cause self-excited instabilities leading to whirling or whipping motion of the shaft centre. This, in turn may create conditions for the development of vaporous cavitation. Brewe used a finite-volume discretization technique to implement the mass conserving Elrod algorithm [**53**] for vaporous cavitation. The solution used the alternating direction implicit (ADI) method to implement a time marching technique; its results compared well with those of Jakobson and Floberg for stationary (gaseous) cavitation [**49**] and reasonably well with those of Jacobson and Hamrock for non-stationary cavitation bubble life [**22**, **23**]. Woods and Brewe [**58**] applied the Elrod algorithm to a theoretical model where vapour cavitation resulted from a dynamic loading situation. The approach accounted for a moving cavitation boundary and ensured the conservation of mass along that boundary, as well as within the cavitated region. The numerical solution used a multigrid iterative technique that yielded good results for both the cavitated and uncavitated regions, while offering significant savings in CPU time when compared to single-grid Gauss–Seidel and direct ADI solutions. Brewe and Jacobson [**59**] also studied numerically the effect of vapour cavitation on vibration amplitude in journal bearings. It is now largely believed that vapour cavitation occurring predominantly in a dynamically loaded bearing is due to the rapid changes in the bearing clearance where the fluid, due to its own inertia, cannot follow the high-frequency motion of the journal, thus causing an instantaneous discontinuity at the solid/fluid interface. This rapid separation causes the local pressure to decrease brusquely and massively, exceeding the yield tensile strength of the fluid and thus inducing flash evaporation. The authors implemented boundary conditions consistent with Elrod's algorithm and performed numerical simulations for eccentricities of $\varepsilon \in (0.1-0.4)$ and 0.4–0.9, respectively. For the first set of instantaneously changing low eccentricities, no vaporous cavitation was obtained. For the second set of instantaneous eccentricities vaporous cavitation occurred 76 per cent of the time. Their numerical results were summarized in computational-based animations which allowed a visual study of the formation and collapse of the vapour bubble. It is apparent that by 1995 the mass-conserving JFO concept and its numerical embodiment into the Elrod algorithm [**53**, **60**] has been adopted as the state-of-the-art for cavitation simulation in hydrodynamic bearings.

In their study of starvation and cavitation in finite-grooved journal bearings, Vincent *et al.* [**61**] made use of both the Elrod algorithm and the improvements offered by Vijayaraghavan and Keith [**54**, **55**]. The 'universal' governing Reynolds equation they proposed, accounts for mass conservation in the cavitation region while including journal rotation and journal centre motion effects. Thus, both static and dynamic cases can be analysed. The finite-difference scheme proposed employs central differencing in the full film area (elliptic nature of the partial differential equation) and upwind in the cavitation region, due to the hyperbolic nature of the differential equation in that region. The numerical solution uses the Gauss–Seidel elimination scheme and, for the dynamic loading case, Booker's mobility method [**62**, **63**]. The authors note in their conclusions that while the Elrod algorithm successfully implements the rupture and reformation boundary conditions for the static case, the mobility method has to be added in the case of dynamic loading where the area occupied by the cavitation zone is not fixed as it changes position from time step to time step.

Paranjpe and Han [**64**] used the mass-conserving Elrod cavitation algorithm [**53**] in the context of a transient thermohydrodynamic analysis of a dynamically loaded journal bearing (engine crankshaft bearings). The finite-volume-based discretization model fully couples the three-dimensional energy equation with the Reynolds equation in its Elrod-modified format. The authors noted that in the dynamic loaded conditions the film thickness as well as the shape and location of the cavitation zone change with time, requiring film grid regeneration at every time step. Ausas *et al.* [**65**] also implemented a mass conserving cavitation algorithm based on the Elrod model. This algorithm was first applied to a vertically oscillating plate, with a prescribed time-dependent change in clearance, and then extended to a dynamically loaded bearing where the film thickness and cavitation location were not *a priori* known. Their contribution is most notable, due to its discretization and the converging method which uses the Newmark scheme, as well as the fact that the code is available as an open source.

In 1988, Booker [**66**] reviewed a series of mathematical models for cavitation implemented through finite-element (FE) algorithms. Although these models have been used extensively, they were not 'flow-preserving', especially in the context of dynamic simulation conditions [**67**]. This lack of mass conservation has been acknowledged as a 'flaw', but was widely practiced because its impact on film thickness and pressure calculations has been found to be minor. Paranjpe and Goenka [**68**] found, however, that this mass conservation violation may have significant effects on both lubricant flow and power dissipation calculations. Kumar and Booker [**67**] proposed a mass-conserving

algorithm for the transient development of cavitation under dynamic conditions based on a FE algorithm developed earlier by Booker and Huebner [**69**] in 1972. This cavitation model presents the FE solution as opposed to its finite-difference (or finite volume) counterpart obtained by Elrod and Adams [**52**], Elrod [**53**], Brewe [**41**], and Vijayaraghavan and Keith [**54**, **55**]. Unlike the Elrod-based algorithms, the Kumar and Booker model assumes the liquid to be incompressible; the cavitated region is treated as compressible, but with the bulk modulus $\beta = 0$. The authors [**67**, **70**] introduce also the notion of a 'biphase', characterized by the following density and viscosity relationships

$$0 \leqslant \rho \leqslant \rho_{\text{liq}} \quad \text{and} \quad 0 \leqslant \mu \leqslant \mu_{\text{liq}}, \quad \text{where} \quad \frac{\rho}{\rho_{liq}} = \frac{\mu}{\mu_{liq}}$$

Under this concept, the film is considered 'complete' when $\rho = \rho_{\text{liq}}$ and $p \geqslant p_{\text{cav}}$. If the pressure–density conditions are at ($p = p_{\text{cav}}$ but $\rho \leqslant \rho_{\text{liq}}$), the film is considered 'incomplete' and containing voids (cavitated structure). The 'complete' film structure is further divided into two types of sub-regions: 'complete-black' ($\rho = \rho_{\text{liq}}, (\partial\rho/\partial t) = 0$) and 'complete-white' regions($\rho = \rho_{\text{liq}}, (\partial\rho/\partial t) \leqslant 0$). Based on the physical observations of the authors, the latter region while still 'complete', is on the verge of cavitating, in effect representing a buffer region that precedes the 'incomplete' film. The Reynolds transient equation

$$\nabla \cdot \left(\frac{\rho h^3}{12\mu} \nabla p \right) = \nabla \cdot (\rho h U) + \frac{\partial}{\partial t(\rho h)}$$

is discretized by means of the Galerkin weighted residuals method into its FE formulation. The velocity U_i, and clearance h_i are defined, while the density ρ_i, viscosity μ_i, and pressure p_i are solved for at each nodal point i. The cavitation algorithm is capable of yielding solutions for both:

(a) specified surface motion;
(b) specified external force type problems.

The authors [**67**, **70**], demonstrated that the mass-conserving formulation simulated well a wide variety of dynamic problems [**71**], and can be readily extended to include axial misalignment and elastic deformation. Kumar and Booker [**71**] further validated their algorithm by comparing its results for a steady-state, non-rotating loaded journal bearing with the quasi-static and dynamic experimental results of Lundholm [**72**]. The cavitation extent and shape calculated by the authors (Fig. 3, [**71**]) compared well with the ones presented by Lundholm. The same algorithm [**71**] was applied to the dynamic simulation of a periodic 'squeeze-driven' flow, for a non-rotating journal bearing carrying a non-rotating sinusoidal load and its results were compared with the experimental results of Phelan [**73**, **74**] . The authors present instantaneous pressure and density distributions for an unwrapped bearing during time sequences when a load reversal takes place. Even though the comparison is not perfectly coincident, it demonstrates that the proposed model is capable of simulating the dominant physical trends. Kumar and Booker have also extended the cavitation FE model to include the energy conservation equation [**75**, **76**]. While recognizing that the heat conduction across the film is important, they chose to neglect the heat transfer to the journal and sleeve. Thus, when integrated across the film of height h, with adiabatic boundary conditions, the model becomes two-dimensional and dominated by advective terms (the velocity vector is $\vec{u} = u\vec{i} + w\vec{k}$, and Φ represents the heat dissipation in the film)

$$\nabla \cdot (\vec{u}\rho c T h) + \frac{\partial(\rho c T h)}{\partial t} = \Phi h$$

Liquid viscosity is assumed to vary with temperature ($\mu/\mu_{\text{o}} = \exp(T_{\text{o}}/T)$), and density variation is treated consistent with the assumptions used by the same authors in references [**67**] and [**70**]. Even though this approach is partially flawed since the journal and sleeve represent important 'sinks' for the frictionally generated heat in the film, the resulting model represents a 'bounding upper limit, for the resulting temperatures. The FE formulation uses the Galerkin method and the overall temperature solution is treated as a time-dependent initial value problem. The results offered by the proposed model are then validated with measured success by comparison with experimental results of Tonnesen and Hansen [**77**], Lund and Tonnesen [**78**] and Ferron *et al.* [**79**].

Boedo and Booker [**80**] applied the mass-conserving FE cavitation algorithm developed by Kumar and Booker [**67**] to a problem characterizing the behaviour of the lubricant film as it was 'negatively' squeezed between parallel, smooth, and rigid surface plates. In this study, they experimented with the determined suitable mesh geometries, allowing both satisfaction of the JFO boundary conditions and the mixed density histories of the spatial and temporal pressure. The methodology identified the full film and cavitation regions as they changed function of the plate position and its velocity. Boedo *et al.* [**81**] continued the work of Kumar and Booker [**67**] by extending their model for smooth surface bearings to incorporate (besides cavitation with mass conservation) bearing material deformation, while allowing fluid density to vary. This elastohydrodynamic (EHD) model provides for the coupling of the FE algorithm with elastic mode shapes where the physical displacements are replaced by generalized modal displacements. The displacements yield a set of transformation relationships accounting for both the elastic displacements and the rigid body motion. This method is then applied to an un-grooved big-end connecting rod bearing. The combination

of the bearing elasticity and mass-conserving cavitation models yielded, over the entire engine cycle, thinner films and higher pressures when compared to a quasi-static model. The choice of mode shapes affected both pressure extrema and the transient performance of the film thickness. Boedo and Booker [**82**] further extended the model presented in reference [**81**] by accounting for structural inertia and surface roughness effects. The geometry involved the tandem of a restrained elastic sleeve and a free rigid journal, with surfaces presenting isotropic roughness with a stochastic distribution [**83**]. The authors modified the Reynolds equation used earlier by Kumar and Booker [**67**] to include flow and roughness factors which depended on the Gaussian roughness distribution [**83**]. In concluding remarks, Boedo and Booker [**82**] reported that when surface roughness and body forces (inertia) are considered, the FE solution of the modified Reynolds equation does well at simulating the following:

(a) bearing elastic deformation;
(b) pressure and oil flows using a linear combination of only a few modes (modes $m = 7$).

Cavitation is accounted for with full mass conservation. While the inertia effects are found to be important, the surface roughness effects seem to be confined to a minor role even when a partial lubrication regime is considered. In a yet further development, Boedo and Booker [**84**] extended their mass-conserving, mode-based EHD FE model [**82**] to a geometry where both the journal (hollow) and the bearing are capable of deforming elastically.

The result trends presented in reference [**82**] were also confirmed by Bonneau *et al.* [**85**] whose EHD analysis of a bearing used a mass conserving cavitation model in combination with structural inertia effects. They [**85**] performed a FE-based EHD analysis for a dynamically loaded automotive connecting rod bearing; the mass-conserving cavitation model was coupled with structural inertia effects. The cavitation zone(s) occurring inside the film are defined by an explicitly stated film rupture and reformation formulation on whose boundaries $p = \mathrm{d}p/\mathrm{d}x = 0$. As this is a dynamically loaded situation, the extent and location of the cavitation zone varies with time. They treated cavitation as a complementary problem using the Murty [**86**] algorithm, and combined it with flow conservation boundary conditions for both the rupture and the reformation zones. Just like Boedo and Booker, they [**85**] concluded that the inertia and elasticity effects are important and, when coupled with the mass-conserving cavitation algorithm, the integrated code enables an optimization process for both the lubricated contact geometry and the location of the supply grooves.

3.4 NSE-based algorithms

All the above discussed methods use the Reynolds equation in conjunction with physical film rupture boundary conditions. However, the fundamental Reynolds equation neglects the inertial terms and the three-dimensional aspects of both the fluid film and the cavity. The computer age has brought about an enormous increase in computational power, and NSE solutions are now a reality. However, the numerical implementation of cavitation algorithms in this environment have also encounterd some significant difficulties. Thus, the large changes in densities, such as those occurring in both the transition to, and within the cavitation zone introduce some numerical handling difficulties (the ratios of $\rho_{\max}/\rho_{\min}$ for boiling/condensing flows are of an order of magnitude of $\mathrm{O}(10^2)$, while for cavitating flows they are of $\mathrm{O}(10^4)$. While in vaporous cavitation a thermodynamic model for vapor generation is arguably available, in the case of gaseous cavitation, where the phenomenon is one of gas diffusion out of the liquid, a model for continuous changing of the gas fraction has not yet been offered. Instead, a fixed gas mass fraction is prescribed, and then allowed to allocate around the bearing based on the pressure distribution. The three dimensionality of the film introduces potential serious memory and algorithm stability problems due to the 'skewness' of the film volume cell, where the thickness of the film is smaller by orders of magnitude (10^{-3}) than the other two dimensions. Last but certainly not least, the already enumerated difficulties are compounded by consideration of inertia introduced non-linearities, and coupling with thermal algorithms and appropriate equations of state. All these make the implementation of a cavitation algorithm a challenging proposition. However, there are numerical NSE solvers able to simulate both the gaseous and vaporous cavitation, as well as a mixture thereof, and define the location and extent of the cavity. The model presented herein authored by the ESI Group [**87**] uses the standard NSE and incorporates variable density capabilities up to ratios of $\rho_{\max}/\rho_{\min} = 5 \times 10^4$. It also uses a multitude of standard turbulence models, among which there are K$-\varepsilon$ and K$-\omega$. The three-dimensional NSE and continuity equations, respectively, are of the general form

$$\frac{\partial}{\partial t}(\rho u_j) + \nabla \cdot (\rho u_j \vec{V}) = -\frac{\partial p}{\partial x_j} + \nabla \cdot (\mu \nabla u_j) + S_j$$

$$\frac{\partial}{\partial t}(\rho) + \nabla \cdot (\rho \vec{V}) = 0$$

where S_j is the source term; when turbulence is considered, S_j incorporates the Reynolds stresses as well. Since the density indicates the state of the cavity content (i.e. vaporous or gaseous), an additional transport equation is needed. This equation is coupled to and

solved simultaneously with the NSE and is written in terms of a new transport variable, the vapour mass fraction, f

$$\frac{\partial}{\partial t}(\rho f) + \nabla \cdot (\rho f \vec{V}) = -\frac{\partial p}{\partial x_j} + \nabla \cdot (\mu \nabla f) + R_e - R_c$$

The terms R_e and R_c represent the evaporation and condensation rates, respectively.

3.4.1 *Vaporous cavitation*

For the case when evaporation occurs due to the pressure falling below the vapour pressure, the R_e and R_c terms become active and take the form of

$$R_e = C_e \frac{V_{ch}}{\sigma} \rho_l \rho_v \sqrt{\frac{2}{3}\frac{(p_{sat} - p)}{\rho_l}}(1 - f);$$

$$R_c = C_c = \frac{V_{ch}}{\sigma} \rho_l \rho_v \sqrt{\frac{2}{3}\frac{(p_{sat} - p)}{\rho_l}}(f)$$

These terms have been derived based on Rayleigh–Plesset ([**36**], chapter 2) equation. This equation accounts for the dynamic expansion or contraction/collapse of a bubble in an infinite liquid field. C_e and C_c represent phase-rate coefficients, σ is the surface tension, and V_{ch} represents a characteristic velocity which in laminar flow cases is set to 1, and in turbulent ones takes the value of the local turbulence intensity. The mixture density is related to the vapour mass fraction by the $\rho - f$ relationship

$$\frac{1}{\rho} = \frac{f}{\rho_v} + \frac{1 - f}{\rho_l}$$

where the subscripts 'v' and 'l' stand for 'vapour' and 'liquid'. Since ρ and f are implicitly contained in terms of the 'f'-transport equation, an iterative computational method combining the NSE with 'f'-transport and $\rho - f$ equations has to be used.

3.4.2 *Gaseous cavitation*

As already discussed, this type of cavitation occurs when non-condensable gases exist in the liquid and when the gas bubble expands or contracts as a function of the environmental pressure. In this case, R_e and R_c are set to $R_e = R_c = 0$. The non-condensable gas mass fraction f is prescribed at the beginning of the calculations and remains constant throughout the calculation (pseudo-cavitation). What changes is the circumferential distribution of the gas mass fraction, f, as it is governed by the three-dimensional pressure distribution. To account for this type of cavitation the same 'f'-transport equation is used, but the expression for the mixture density, ρ, is different

$$\frac{1}{\rho} = \frac{f_v}{\rho_v} + \frac{f_g}{\rho_g} + \frac{1 - f_v - f_g}{\rho_l}$$

In this case, $f_v = 0$ and the density of the gas ρ_g is calculated from an equation of state, most often the ideal gas law

$$\rho_g = \frac{w_{mol} p_{sat\,gas,i}}{RT}$$

where w_{mol} is the molecular weight of the gas and $p_{sat\,gas,i}$ is the saturation pressure of the gas in the liquid. Note that while the above equation allows the calculation of the mixture density for the simultaneous occurrence of both vaporous and gaseous cavitation; the amount of non-condensable gases remains fixed throughout the calculations.

4 EXPERIMENTAL EVIDENCE

There is a rather extensive body of literature dealing with the experimental visualization of cavitation and associated pressures. For a more complete historical perspective, the reader is referred again to Dowson *et al.* [**13**] and Brewe *et al.* [**14**], which represent seminal collections of symposia papers dealing with the topic during the 1970s and 1980s. Experimental evidence shows that both gaseous and vaporous cavitation may occur in bearings, separately, or in conjunction with each other. Cavitation may develop under steady or dynamic loading, and its characteristics and basic phenomenological aspects have been studied for many decades. The onset criteria, the cavitation bubble content, its general physical behaviour [**15**], and effect on the bearing dynamics are still of major interest.

As discussed earlier [**19**], the theoretically calculated time constant of vaporous cavitation has proven to be much shorter than that of the gaseous one. As a result, the argument is often made that the process of cavitation is mostly vaporous in nature, since gas diffusion takes a longer time to occur. Work done by Jacobson and Hamrock, published in 1983 [**22**, **23**], concentrated on the visualization of flow between a rotating journal and a stationary transparent cylindrical sleeve. The journal could be shifted away from the sleeve, thus being able to rotate about the journal-sleeve axis in a 'centred', or 'non-centred' whirl (static or dynamic eccentricity, respectively). This motion was obtained by using a shaft that could rotate around its own centre and be supported by a ball bearing that could vibrate in circular motion around the static centre. The authors used high-speed photography to record and confirm the appearance, development, and disappearance of the cavitation bubble. They concluded that under dynamic loading not only did gaseous cavitation ensue but also 'previously unsuspected vapour cavitation' was also present. It was found that gaseous cavitation increased with time, but after 'many hundreds of pressure cycles', the cavitation bubble volume became constant. By contrast, the vapour cavitation

bubbles were observed to 'collapse at pressures lower than the atmospheric pressure'. In support of their hypothesis [**19**], where different time constants are associated with vaporous and gaseous cavitation, Sun and Brewe [**18**, **21**] present experimental results regarding the development of vaporous cavitation for a dynamically loaded journal bearing. Their work, in fact, continued the earlier work of Jacobson and Hamrock [**22**, **23**]. Suspecting that the material of the transparent sleeve used in references [**22**] and [**23**] was compliant and deformed elastically with pressure, Sun and Brewe replaced it with a quartz sleeve that could perform a whirling motion. They used the same photographic set-up as in references [**22**] and [**23**], with camera speeds of 2000 fps and shutter speeds as small as 2×10^{-4} s. It was found that the cavitation pattern was dependent on bearing clearance and eccentricity, as well as whether the whirl was 'centred' or 'non-centred'. During the 'centred' whirl, the lubricant cavitated locally with the bubble revolving in synchronization with the whirling sleeve. During the 'non-centred' whirl, the cavitation bubble formed 'amidst the fluid film', grew to a peak size, then shrank and collapsed. The authors state that it was not possible to visually determine whether the content of the bubble was vapour, gas, or a mixture thereof.

It is well known that vaporous cavitation is associated with the damage that implosion or collapse of the cavitation bubble leaves behind it. This type of damage is not unlike the damage witnessed on ships' propellers caused by the cavitation formed in the blade's wake. According to Wilson [**25**], damage caused by the collapse of the bubble exposes a rough material texture, but if microscopic particles are trapped in the damage 'crevices' they can further erode these surfaces giving them a polished appearance. Relatively high local temperatures and pressures associated with the bubble collapse may cause chemical reactions between the bearing surface and the lubricant, initiating subsequent corrosion. These reactions may accentuate the damage caused initially by the collapsing bubble. Wilson further noted that the cavitation damage occurs primarily in the unloaded areas of the bearing and may be caused either by the following:

(a) flow of fluid under special conditions or;
(b) externally imposed fluctuating loads.

With regard to (a), Campbell [**88**] notes that cavitation damage may occur due to four different causes: suction, discharge, sudden pressure fluctuations, and impact. According to Blok [**89**], the internal heating due to intense viscous shearing in full EHD films may cause thermal instabilities that are also responsible for the initiation of cavitation. Its subsequent violent collapse may be the cause of the 'scuffing' of the rubbing surfaces. This type of cavitation is, according to Blok, of a 'novel, thermally explosive kind' that is characterized by film implosion. Blok offers further a mathematical model supporting his theory.

Other experimental work demonstrating, under steady-state conditions, the stability of the cavitation zone (see references [**15**] and [**16**]) and lack of pitting damage supports the notion that cavitation, when it occurs in bearings, is mostly gaseous: the gas saturation pressure in the oil is always reached long before the vapour pressure (see Fig. 1, and Table 1), while pre-existing dissolved gas micro-bubbles serve as initial cavitation promoters. In a 1979 review paper, Dowson and Taylor [**20**] presented extensive experimental proof of gaseous cavitation with visual evidence of gas bubbles and their formation in the divergent region of a lubricant film. In this context, they also discussed the propriety of rupture and reformation boundary conditions and cited pertinent work done by Makenham [**90**] who visualized the formation of gas fingers in the thick film region of a reversed stepped parallel-surface slider bearing. Makenham also reported that the number of gas fingers increased with the sliding speed until they coalesced into a single, all encompassing bubble. A similar phenomenon where individual bubbles grow and coalesce as speed increases has been documented by Xing [**17**] in a cylindrical geometry of a two-phase squeeze film damper (Fig. 9). In this figure, the motion is from bottom-to-top and both the film rupture and its reformation are clearly evident. The three sequences (a, b, c) represent time snapshots of the cavity development at 700, 1500, and 3000 r/min, respectively.

The fluid used in the experiment which generated Fig. 9 has a dynamic viscosity of 20cP. In Fig. 9(a), at the lower speed of 700 r/min, the fluid has already ruptured and fern leaf structures representing the incipience of the cavitation zone are clearly visible at the beginning of the divergent zone. Finger and fluid rupturing (or cracking) structures are also present in the divergent region with the reformation boundary distinctly visible. In Figs 9(b) and 9(c) one can see the shape and structure of the cavitation zone as the velocity is increased to 1500 and 3000 r/min, respectively. In Fig. 9(b), discrete small gas bubble formations are sharply defined together with the boundary of the cavity and its reformation tip. In Fig. 9(c), as the shaft speed was increased to 3000 r/min, the bubbles have multiplied significantly, while decreasing in size and starting to coalesce towards the cavitation boundary reformation tip. Based on the visual appearance of the tip region, one can surmise the existence of some vapour mixed with gas as well.

Figure 10 presents experimental results for the development of the gaseous cavitation region in a submerged journal bearing in steady-state operation (see also reference [**91**]). Figures 10(a) and (b) present the downstream cavitation region at two different angles around the circumference, for a fixed velocity of 2000 r/min. The contour of the cavity and its

reformation region are well defined, while some gas bubble shedding occurs at the reformation tip. The cavitation zone is relatively small with a reduced size tip area by comparison to the ones shown in Figs 10(c) and (d), where the journal rotates at 6000 r/min. In the latter case, the cavitation zone has increased considerably both axially and circumferentially, its reformation tip has extended and is located further downstream in the divergent zone. For the same submerged bearing Figs 10(e) to (g) present the incipient cavitation formation evident during start-up when shear combined with subatmospheric pressures, cause the initial film rupture. These fern-leaf formations are identical in structure to those observed in Fig 9(a), for the case of the two-phase squeeze film damper. Figure 11 is related to the experimental findings of Fig. 10 and presents the reconstruction of the pressure maps for the cavitation zones shown by Figs 10(a) to (d), respectively. The experimental pressures were collected by means of a specially designed pressure sensor, located in the mobile transparent external sleeve that could travel both axially and circumferentially relative to the position of the cavitation zone. The three-dimensional results $p = p(x, y)$ display the extent of the zone for both the 2000 and 6000 r/min cases. A study of the associated contour maps reveals that the pressure magnitudes in the cavitation region are moderately subatmospheric giving credence to the hypothesis supported by the data presented by Table 1 (i.e. vaporous cavitation appears only at extremely low subatmospheric pressures).

Etsion and Ludwig [**92**] visualized the cavitation zone of a submerged journal bearing operating under steady-state conditions. The pressure measurements made by means of a travelling pressure transducer showed that the lowest found pressures were about 67 kPa (roughly 34 kPa below atmospheric), when the operating speed was 3000 r/min. The authors concluded that since the vapour pressure for the oil was about 0.1 mmHg (0.013 kPa), the cavity was gaseous in nature. Their determination was later confirmed by means of a mass spectrometer, which demonstrated that the cavity contained no oil vapour. Braun and Hendricks [**91**] performed experiments similar to those of Etsion and Ludwig, and visualized the three dimensionality of the cavity. The authors [**91**] used a modified miniature travelling sensor where the pressure probe was combined with a thermocouple thus gaining the capability to measure simultaneously the pressure and temperature at the same location. It was shown that the pressure is not constant in the cavitation zone (as assumed by most numerical models), as it varies with the circumferential and axial positions in the zone and is only moderately subatmospheric. The associated temperatures were well below the saturation temperatures corresponding to the measured pressures. Based on flash calculations which determine the percentage of the gas mixture released from the oil solution at a given pressure and temperature, they reached the conclusion that the content of the cavity was gaseous. In that respect, Braun and Hendrick's findings reinforce those of Etsion and Ludwig [**92**] and Dowson and Taylor [**16**]. Similar to the findings offered in references [**16**], [**91**], and [**92**], Groper and Etsion [**93**] also observed non-constant subatmospheric pressures in the cavity zone and investigated two possible mechanisms as follows.

1. The shear of the cavity gas bubble by the thin lubricant film dragged through the cavitation zone by the rotating shaft.
2. The mass transfer mechanism which dictates the rate of diffusion of dissolved gas in and out of the lubricant.

They found that the cavitation shape was fairly well predicted by the 'shear' mechanism, but the measured pressures were not consistent with the model prediction. They concluded that the mass transfer mechanism effects on the pressure build-up in the cavitation zone can be completely ignored. In a later study [**94**], the same authors determined that the pressure build-up, particularly towards the end of the cavitation zone can be fairly well predicted by including the reverse flow, previously observed in the experimental works performed by Etsion and Ludwig [**92**] and by Heshmat and Pinkus [**95**].

If falling pressures in the bearing divergent zone reach below the gas saturation pressures, the vapour pressure threshold is breached (see Fig. 2) and vapour is also released into the bubble. At this point, gas and vapour coexist and only precise knowledge of the state equation $p = f(T)$ for the component hydrocarbons will tell what sort of cavitation takes place (cavitation, vaporous, or mixed). As discussed, it has been predicted theoretically and proven experimentally that in the case of dynamically loaded journal bearings, or in squeeze-film dampers, the transition to the extremely low vapour pressures (short time constant [**19**], happens so rapidly that the fluid, due to its mass inertia, cannot follow the journal motion.

In the early 1960s, Hays and Feiten [**96**] performed a study of a cavity formation and growth when two flat parallel plates separated by a thin fluid film are pulled apart from each other. Their experiment is probably an excellent of *in situ* example where the fluid in isolation, due to a sudden mechanical perturbation, fails to follow the moving solid boundary. The authors also proposed an analytical model for the formation of the cavity. They noted that while the equations simulating the process are not difficult to establish, the actual solution is difficult to obtain, due to the appearance of a moving 'free boundary'. Thus, the necessity of 'well-set' boundary conditions dominates the conceptual effort of obtaining proper solutions. Hays and Feiten constructed a device formed of a circular upper

plate that was optically flat, while its lower counterpart was made out of polished steel. The experimental procedure consisted of pulling abruptly and instantly the optical plate away from the steel one, while a high-speed camera was recording the rupture of the liquid film and subsequent formation of the voids. The resulting photographs, are described as presenting:

> …three distinct periods of cavity growth. First there is a period of nucleation when many small cavities are seen to form in an apparently random pattern over the film extent…(followed by) an extremely interesting but complex growth phenomenon which is characterized by a fracturing of the advancing cavity front…During this growth phase many fern-like structures form and migrate…The final (third) stage is one of coalescence, a single cavity being formed which then collapses…

A mathematical model is also offered with the following observation:

> …we are initially faced with the problem of determining the physical nature of the flows about the cavities…. The second problem which has been discussed by Birkoff [**11**] is related to the nature of the liquid-gas interface, this being a free boundary…

In the 1970s and 1980s, experimental work has been reproduced by other researchers, under the same or

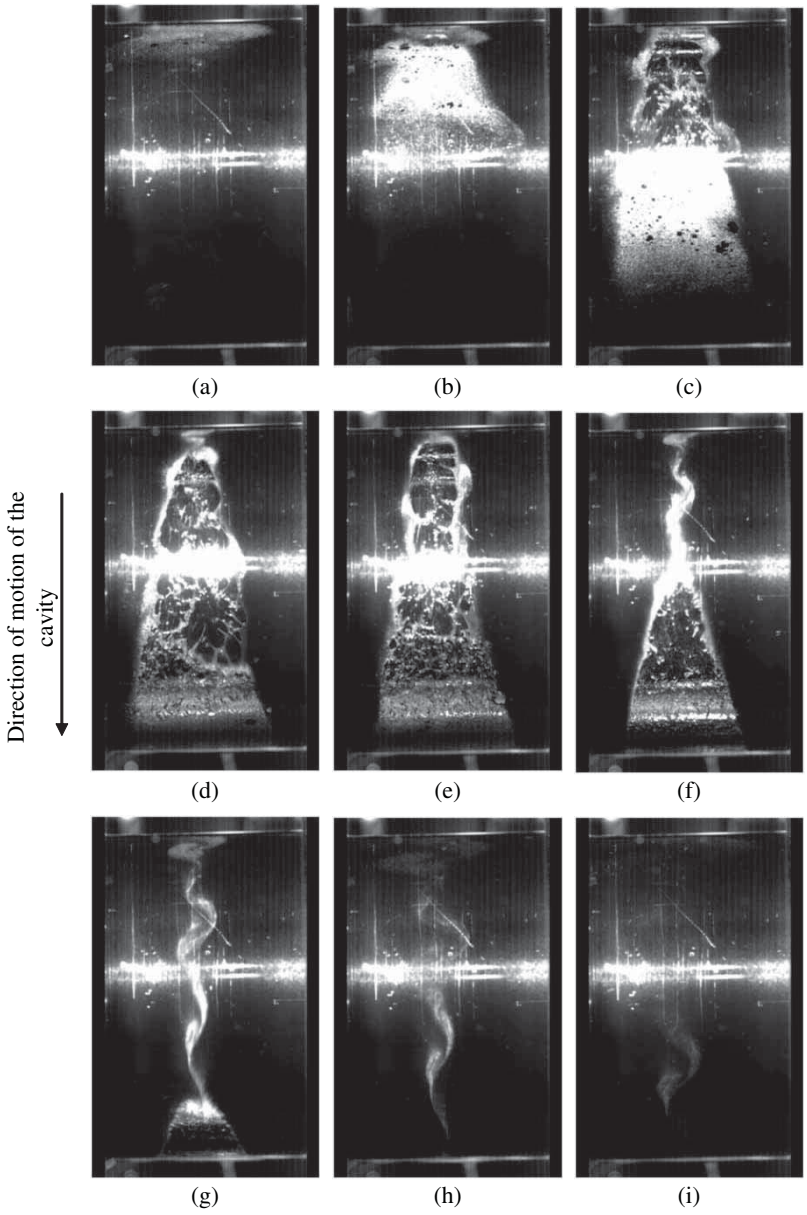

Fig. 12 Travelling cyclic vaporous cavitation. The window of observation is Eulerian in nature: over one cycle, one can observe the entire cavity from rupture to reformation. The angular speed is 3500 r/min, and the equivalent rotor diameter is 78.75 mm

different circumstances (as it will shown below). However, from the theoretical point of view even though today there are algorithms that do a fair job at predicting the film rupture, formation, and reformation, an ultimate exact model that dynamically accounts for both gas and vapour nucleation, continuous generation, and eventual collapse is still missing.

Through Frenkel theory [**30**], and also as mentioned by Brennen [**36**], it was postulated that a dearth of cavitation promoters in the fluid leads to relatively strong tensile stresses causing a metastable state, from where transition may occur spontaneously to vapour (Fig. 2) (the direct transition from 2′ to 4 is akin to liquid flashing). In such a case, a vaporous dynamic cavitation situation ensues before non-condensable gas may be released from the oil. Wilson [**25**] and then Berthe [**97**] present proof of vaporous cavitation by showing photographic evidence of damage in journal bearings, consistent with the type of damage observed on ship propellers, which undoubtedly is produced by vaporous cavitation in water.

Figure 12 presents evidence of vaporous cavitation for a travelling cavitation zone. The sequence of pictures shows the extent of the cavity around the shaft of a squeeze film damper [**17**]. The window of observation is Eulerian in nature, and due to the travelling characteristic of the cavitation bubble, over one cycle one can observe the entire cavity from rupture to reformation. The individual frames were 'time-stopped' and recorded by means of a high-speed video camera operating at the rate of 10 000 frames/s. Each frame sequentially presents a position of the cavity zone as it travelled around the circumference. In Fig. 12(a), one can view at the top of the image the bottom of the cavity entering the viewing area. Figures 12(b) and (c) show the bottom cavitation zone advancing in the field of view with individual gas bubbles visible at the bottom of Fig. 12(c). These bubbles are similar in structure and appearance to those presented in Figs 9(b) and 9(c). Finally, at the upper portion of the cavity, with its reformation zone travelling through the viewing window (Figs 12(d) and (e), one can see the 'explosive' and chaotic nature of its content. In this area, the small individual gas bubbles have probably coalesced and mixed with explosive (flash evaporation) release of vapour. The sudden powerful evaporation process is most probably responsible for the chaotic aspect of the cavity. Finally, Figs 12(f) to (h) present the reformation tip of the cavity as it travels out of the field of view. The vapor shedding and/or gas bubbles are visible in Figs 12(g) and (h) and are similar to the shedding observed in Figs 10(c) and (d) for the submerged journal bearing. The similarity between the visual aspect of the reformation tips for a submerged bearing and a squeeze film damper bear testimony to the similar process of gas and vapour generation as the pressures become subatmospheric.

5 SUMMARY

Even though the list of references associated with this review is rather extensive, in no way does it exhaust the vast literature dedicated to the study of cavitation. The intent was to summarize the following:

(a) advances in analytical and numerical modelling;
(b) draw attention to the thermodynamic aspects of cavitation;
(c) do so while reflecting on physical or experimental observations.

To conclude, the authors would like to note the following.

1. Liquids can, in general, withstand relatively high tensile stresses ('negative pressures'). The limiting yield stress depends on the level of nucleation sites (whether these sites are impurities in the mating solid or the liquid itself), as well as on the dynamics of a bearing system.
2. Gaseous cavitation is governed by lubricant chemistry and by the ensuing trapped gas partial saturation pressures and temperatures. Changes in the bearing environment, lubricant shear rates, and heat dissipation, all affect the number and size of the nuclei that promote cavitation.
3. Vaporous, just like gaseous, cavitation is due to a fracture of the fluid; however, the former type of cavitation, unlike the latter, is induced by an abrupt phase change. This is most likely the result of a thermodynamic metastable phenomenon occurring during transient dynamic events.
4. Experimental evidence draws attention to significant similarities between classical solid fracture mechanics and cavitation.
5. As early as 1904 (Sommerfeld) and 1914 (Gumbel), cavitation has been recognized as an important 'game changing' phenomenon in bearing modelling. The challenges in incorporating cavitation in the thermo-fluid model are rooted in the ability to respect the conservation of mass throughout the bearing including at the liquid–cavity interface. The early cavitation models of Sommerfeld, Gumbel, and Swift–Stieber did not rigorously respect mass continuity. More recent attempts, pioneered through the JFO model, the Elrod algorithm, Vijayaraghavan *et al.*, Booker, Kumar *et al.*, and Boedo *et al.* have offered both analytical and numerical contributions that strictly respected mass continuity. In the overall context, it was noted that the earlier (non-mass-conserving) models yielded good results for pressure and film thickness measurements. As Paranjpe *et al.* [**64**] observed, it was only in the calculation of the thermal performance and power consumption that mass conserving versus non-mass-conserving cavitation algorithms yielded widely different results.

6. The computer age has removed countless modelling limitations. This has led to more and more frequent attempts to replace the two-dimensional Reynolds equation with the fully populated three-dimensional NSE. A three-dimensional computational venue permits the quantification of inertial effects and can model:
   (a) gaseous cavitation;
   (b) vaporous cavitation;
   (c) a mixture thereof.
7. Modern experimental work has been used to advance the understanding of the physical characteristics of the cavitation zone and validate both finite-difference (volume) and FE algorithms.

REFERENCES

1 **Reynolds, O.** On the theory of lubrication and its application to Mr. Beauchamp Tower's experiments including an experimental determination of the viscosity of olive oil. *Philos. Trans. R. Soc. A*, 1886, **177**, 157.
2 **Sommerfeld, A.** Zur hydrodynamische theorie der schmiermittelreibung. *Zeit Math. Phys.*, 1904, **50**, 97–155.
3 **Bertholet, M.** Sur quelques phenomenes de dilation forcee des liquides. *Ann. Chim. Phys.*, 1850, **30**, 232–235.
4 **Reynolds, O.** On the internal cohesion of liquids and the suspension of a column of mercury to a height more than double that of the barometer. *Manchester Literary and Phil. Soc. Proc (and Manchester Literary and Phil. Soc. Memoirs)*, 1878 (and 1882), **17 (and 7)**, 159–175 (and 1–19).
5 **Davies, R.** *Cavitation in real liquids*, 1964 (GM Research Labs, Warren, Michigan; Elsevier Publishing Co., New York).
6 **Plesset, M. S.** Bubble dynamics. In *Cavitation in real liquids*, 1964, pp. 1–19 (GM Research Labs, Warren, Michigan; Elsevier Publishing Co, New York).
7 **Westwater, J. W.** Measurements of bubble growth during mass transfer. In *Cavitation in real liquids* (Ed. R. Davies), 1964, pp. 34–55 (GM Research Labs, Warren, Michigan; Elsevier Publishing Co., New York).
8 **Prigogine, I.** The molecular theory of surface tension. In *Cavitation in real liquids* (Ed. R. Davies), 1964, pp. 147–163 (GM Research Labs, Warren, Michigan; Elsevier Publishing Co., New York).
9 **Benjamin, T. B.** Surface effects in non-spherical motions of small cavities. In *Cavitation in real liquids* (Ed. R. Davies), 1964, pp. 164–180 (GM Research Labs, Warren, Michigan; Elsevier Publishing Co., New York).
10 **Taylor, G. I.** Cavitation in hydrodynamic lubrication. In *Cavitation in real liquids* (Ed. R. Davies), 1964, pp. 80–101 (GM Research Labs, Warren, Michigan; Elsevier Publishing Co., New York).
11 **Birkhoff, G.** Free boundary problems for viscous flow in channels. In *Cavitation in real liquids* (Ed. R. Davies), 1964, pp. 102–122 (GM Research Labs, Warren, Michigan; Elsevier Publishing Co., New York).
12 **Floberg, L.** Cavitation in lubricating oil films. In *Cavitation in real liquids*, 1964, pp. 138–146 (GM Research Labs, Warren, Michigan, Elsevier Publishing Co., New York).
13 **Dowson, D., Godet, M.,** and **Taylor, C. M.** Cavitation and related phenomena in lubrication (Eds D. Dowson, M. Godet, and C. M. Taylor). In Proceedings of the 1st Leeds–Lyon Symposium on *Tribology* (Eds D. Dowson, M. Godet, and C. M. Taylor), University of Leeds, Leeds, UK, 1974, pp. 1–238 (Mechanical Engineering Publications Ltd, London, UK).
14 **Brewe, D. E., Ball, J. H.,** and **Khonsari, M. M.** Introduction. Part 2: current research in cavitating fluid films. In Proceedings of the Cavitation Symposium, STLE Annual Meeting, NASA TM-103184, 1988, pp. 25–26.
15 **Swales, P. D.** A review of cavitation phenomena in engineering situations. In *Cavitation and related phenomena in lubrication* (Eds D. Dowson, M. Godet, and C. M. Taylor), Proceedings of the 1st Leeds–Lyon Symposium on *Tribology*, University of Leeds, Leeds, UK, 1974, pp. 3–9 (Mechanical Engineering Publications Ltd, London, UK).
16 **Dowson, D.** and **Taylor, C. M.** Fundamental aspects of cavitation in bearings. In *Cavitation and related phenomena in lubrication* (Eds D. Dowson, M. Godet, and C. M. Taylor), Proceedings of the 1st Leeds–Lyon Symposium on *Tribology*, University of Leeds, Leeds, UK, 1974, pp. 15–25 (Mechanical Engineering Publications Ltd, London, UK).
17 **Xing, C.** Analysis of the characteristics of a squeeze film damper by threedimensional Navier–Stokes equations. In *Mechanical engineering*, 2009, pp. 456, 500 (University of Akron, Akron).
18 **Sun, D. C.** and **Brewe, D. E.** A high speed photography study of cavitation in a dynmically loaded journal bearing. *J. Tribol.*, 1991, **113**(2), 287–294.
19 **Sun, D. C.** and **Brewe, D. E.** Two reference time scales for studying the dynamic cavitation of liquid films. *J. Tribol.*, 1992, **114**(3), 612–615.
20 **Dowson, D.** and **Taylor, C. M.** Cavitation in bearings. *Annu. Rev. Fluid Mech.*, 1979, **11**, 35–66.
21 **Sun, D. C., Brewe, D. E.,** and **Abel, P. B.** Simultaneous pressure measurement and high-speed photography study of cavitation in a dynamically loaded journal bearing. *J. Tribol.*, 1993, **115**(1), 88–95.
22 **Jacobson, B. O.** and **Hamrock, B. J.** Vapour cavitation in dynamically loaded journal bearings. In *NASA TM-83366*, 1983, 14 pp. (NASA Lewis (Glenn) Research Center).
23 **Jacobson, B. O.** and **Hamrock, B. J.** High-speed motion picture camera experiments of cavitation in dynamically loaded journal bearings. *J. Lubric. Tech.*, 1983, **105**(3), 446–452.
24 **Jacobson, B.** Cavitation in journal bearings and squeeze-film dampers: analytical. In *Current research in cavitating fluid films* (Eds D. E. Brewe, J. H. Ball and M. M. Khonsari), 1988, pp. 54–56 (NASA Technical Memorandum 103184, Cleveland, Ohio)
25 **Wilson, R. W.** Cavitation damage in plain bearings. Cavitation and related phenomena in lubrication. In Proceedings of the 1st Leeds–Lyon Symposium on *Tribology*, University of Leeds, Leeds, UK, 1974, pp. 177–184.
26 **Temperley, H. N. V.** The tensile strength of liquids. In *Cavitation and related phenomena in lubrication* (Eds D. Dowson, M. Godet, and C. M. Taylor), Proceedings of the

1st Leeds–Lyon Symposium on *Tribology*, 1974, pp. 11–14 (Mechanical Engineering Publications Ltd, London, UK).
27 **Temperley, H. N. V.** and **Chambers, L. G.** The behaviour of water under hydrostatic tension: part I. *Proc. Physical Soc.*, 1946. **58**(4), 420–436.
28 **Temperley, H. N. V.** The behaviour of water under hydrostatic tension: part II. *Proc. Physical Soc.*, 1946, **58**(4), 436–443.
29 **Fisher, J. C.** The fracture of liquids. *J. Appl. Phys.*, 1948, **19**(11), 1062–1067.
30 **Frenkel, J.** *Kinetic theory of liquids*, 1955 (Dover Publications, New York).
31 **Volmer, M.** *Kinetik der phasenbildung*, 1939 (Theodor Steinkopff, Dresden and Leipzig).
32 **Hendricks, R. C., Mullen, R. L.,** and **Braun, M. J.** Analogy between cavitation and fracture mechanics. In *NASA Lewis RC*, TM 83071/1983 (26 pages) and Proceedings of the ASME/JSME Thermal Engineering Conference, 1983, vol. 1, pp. 35–43.
33 **Griffith, A. A.** Phenomena of rupture and flow in solids. *Philos. Trans. R. Soc., Lond. A*, 1921, **221**, 163–198.
34 **Hoffman, R. D.** and **Myers, R. R.** The splitting of thin liquid films. II. Cavitation dynamics. *Trans. Soc. Rheol.*, 1962, **6**, 197–207.
35 **Floberg, L.** *On the tensile strength of liquids*, 1973, pp. 1–13 (Transactions of Machine Elements Division, Lund Technical University, Lund, Sweden).
36 **Brennen, C. E.** *Cavitation and bubble dynamics*, 1995. The Oxford engineering science series (Oxford University Press, Oxford).
37 **Gumbel, L.** Das Problem der Lagerreibung. *Mon. Berl. Bezirksverein., V.D.I.*, 1914, **5**, 87–104 and 109–120.
38 **Swift, H. W.** The stability of lubricating films in journal bearings. *Proc. Inst. Civil Engnrs (Lond.)*, 1932, **233**, 267–288.
39 **Stieber, W.** *Das schwimmlager: Hydrodynamische Theorie des Gleitlagers*, 1933, 106 p. (V.D.I. Verlag GMBH, Berlin).
40 **Floberg, L.** On journal bearing lubrication considering the tensile strength of the liquid lubricant. In Transactions of the Machine Elements Division, Lund Technical University, Lund, Sweden, 1973, p. 1–26.
41 **Brewe, D. E.** Theoretical modeling of the vapor cavitation in dynamically loaded journal bearings. *J. Tribol.*, 1986, **108**(4), 628–638.
42 **Floberg, L.** Sub-cavity pressures and number of oil streamers in cavitation regions with special reference to the infinite journal bearing. *Acta Polytech. Scand. Mech. Engng Ser.*, 1968, **37**, 1–31.
43 **Floberg, L.** On hydrodynamic lubrication with special reference to sub-cavity pressures and number of streamers in cavitation regions. *Acta Polytech. Scand., Mech. Eng. Ser.*, 1965, **19,** 1–35.
44 **Mori H., Yabe, H.,** and **Fujita, Y.** On the separation boundary conditions for fluid lubrication theories of journal bearing. *ASLE Trans.*, 1968, **11**, 196–203.
45 **Hopkins, M. R.** Viscous flow between rotating cylinders and a sheet moving between them. *Br. J. Appl. Phys.*, 1957, **8**, 442–447.
46 **Birkhoff, G.** and **Hays, D. F.** Free boundaries in partial lubrication. *J. Math. Phys.*, 1963, **42**(2), 126–138.
47 **Coyne, J. C.** and **Elrod Jr, H. G.** Conditions for the rupture of a lubricating film, part I: theoretical model. *J. Lubric. Technol.*, 1970, **92**(July), 451–456.
48 **Coyne, J. C.** and **Elrod Jr, H. G.** Conditions for the rupture of a lubricating film, part II: new boundary conditions for reynolds' equation. ASME paper 1970, p. 70-Lub-3.
49 **Jakobson, B.** and **Floberg, L.** *The finite journal bearing considering vaporization*. Transactions of Chalmers University Technology, Goteborg, Sweden, 1957, vol. 190, 1–119.
50 **Olsson, K. O.** *Cavitation in dynamically loaded bearings*. Transactions of Chalmers University Technology, Goteborg, Sweden, 1965, vol. 308.
51 **Floberg, L.** Cavitation boundary conditions with regard to the number of streamers and tensile strength of the liquid. In *Cavitation and related phenomena in lubrication*, Proceedings of the 1st Leeds–Lyon Symposium on *Tribology*, University of Leeds, Leeds, UK, 1974, pp. 31–36 (Mechanical Engineering Publications Ltd, London, UK).
52 **Elrod, H. G.** and **Adams, M. L.** A computer program for cavitation and starvation problems. In *Cavitation and related phenomena in lubrication*, Proceedings of the 1st Leeds–Lyon Symposium on *Tribology*, University of Leeds, Leeds, UK, 1974 (Mechanical Engineering Publications Ltd, London, UK).
53 **Elrod, H. G.** A cavitation algorithm. *J. Lubr. Technol.*, 1981, **103**(3), 350–354.
54 **Vijayaraghavan, D.** and **Keith Jr, T. G.** Development and evaluation of a cavitation algorithm. *Tribol. Trans.*, 1989, **32**(2), 225–233.
55 **Vijayaraghavan, D.** and **Keith Jr, T. G.** An efficient, robust, and time accurate numerical scheme applied to a cavitation algorithm. *J. Tribol.*, 1990, **112**(1), 44–51.
56 **Vijayaraghavan, D.** and **Keith Jr, T. G.** Grid transformation and adaptation techniques applied in the analysis of cavitated journal bearings. *J. Tribol.*, 1990, **112**, 52–59.
57 **Vijayaraghavan, D.** and **Keith Jr, T. G.** Analysis of a finite grooved misaligned journal bearing conisdering cavitation and starvation effects. *J. Tribol.*, 1990, **112**(1), 60–67.
58 **Woods, C. M.** and **Brewe, D. E.** The solution of the Elrod algorithm for a dynamically loaded journal bearing using multigrid techniques. *J. Tribol.*, 1989, **111**(2), 302–308.
59 **Brewe, D. E.** and **Jacobson, B. O.** The effect of vibration amplitude on vapour cavitation in journal bearings. *Wear*, 1987, **115**(1–2), 63–73.
60 **Adams, M. L.** The influence of cavitation on journal-bearing. In *Current research in cavitating fluid films*, (Eds D. E. Brewe, J. H. Ball, and M. M. Khonsari), 1988, pp. 52–53 (NASA Technical Memorandum 103184, Cleveland, Ohio).
61 **Vincent, B., Maspeyrot, P.,** and **Frene, J.** Starvation and cavitation effects in finite Grooved Journal Bearing. *Tribol. Ser.* 1995, **30**, 455–464.
62 **Booker, J. F.** Dynamically loaded journal bearings: mobility method of solution. *Trans. ASME, D, J. Basic Engng*, 1965, **87**(3), 537–546.
63 **Booker, J. F.** Dynamically loaded journal bearings: numerical application of the mobility method. *Trans. ASME, J. Lubr. Technol.*, 1971, **93**, 168–176 (*Errata*, 1972, **94**, 315).
64 **Paranjpe, R. S.** and **Han, T.** A transient thermohydrodynamic analysis including mass conserving cavitation for dynamically loaded journal bearings. *J. Tribol.*, 1995, **117**(2), 369–378.

65 **Ausas, R. F., Jai, M.,** and **Buscaglia, G. C.** A mass-conserving algorithm for dynamical lubrication problems with cavitation. *J. Tribol.*, 2009, **131**.

66 **Booker, J. F.** *Classic cavitation models for finite element analysis*. In *Current research in cavitating fluid films* (Eds D. E. Brewe, J. H. Ball, and M. M. Khonsari), 1988, pp. 39–40 (NASA Technical Memorandum 103184, Cleveland, Ohio).

67 **Kumar, A.** and **Booker, J. F.** A finite element cavitation algorithm. *J. Tribol.*, 1991, **113**(2), 276–286.

68 **Paranjpe, R. S.** and **Goenka, P. K.** Analysis of crankshaft bearings using a mass conservation algorithm. *STLE Tribol. Trans.*, 1990, **33**(3), 333–344.

69 **Booker, J. F.** and **Huebner, K. H.** Applications of finite element methods to lubrication: an engineering approach. *ASME J. Lubr. Technol.*, 1972, **94**(4), 313–323.

70 **Kumar, A.** and **Booker, J. F.** Mass-conservative cavitation analysis for engine bearings, In Proceedings of the 17th Leeds–Lyon Symposium on *Tribology: vehicle tribology*, 1991, 27–32 (Elsevier, Amsterdam).

71 **Kumar, A.** and **Booker, J. F.** A finite element application algorithm: application/validation. *J. Tribol.*, 1991, **113**(2), 255–261.

72 **Lundholm, G.** The circumferential groove journal bearing considering cavitation and dynamic stability. *Acta Scand.*, 1969, **42** (ME Series, Stockholm).

73 **Phelan, R. M.** The design and development of a machine for the experimental investigation of dynamically loaded sleeve bearings. In M.E. Department, Master M.E., 1950 (Cornell University Press, Ithaca, New York).

74 **Phelan, R. M.** Non-rotating journal bearings under sinu-soidal loads. In Proceedings of the ASME Lubrication Symposium, Miami, Florida, 8–9 May 1961, paper 61-LubsS-6.

75 **Kumar, A.** and **Booker, J. F.** Cavitation and thermal effects in journal bearing application. In Proceedings of the Japan International Tribology Conference, 1990, vol. 3, 1491–1496.

76 **Kumar, A.** and **Booker, J. F.** A mass and energy conserving finite element lubrication algorithm. *J. Tribol.*, 1994, **116**, 667–671.

77 **Tonnesen, J.** and **Hansen, P. K.** Some experiments on the steady-state characteristics of a cylindrical fluid film bearing considering thermal effects. *ASME J. Lubr. Technol.*, 1981, **103**, 107–114.

78 **Lund, J. W.** and **Tonnesen, J.** An approximate analysis of the temperature conditions in a journal bearing. Part II: application. *ASME J. Lubr. Technol.*, 1984, **106**, 237–245.

79 **Ferron, J., Frene, J.,** and **Boncompain,R.** A study of the thermohydrodynamic performance of a plain journal bearing: comparison between theory and experiments. *ASME J. Lubr. Technol.*, 1983, **105**, 422–428.

80 **Boedo, S.** and **Booker, J. F.** Cavitation in normal separation of square and circular plates. *J. Tribol.*, 1995, **117**(3), 403–410.

81 **Boedo, S., Booker, J. F.,** and **Wilkie, M. J.** A mass conserving modal analysis for elastohydrodynamic lubrication. In Proceedings of the 21st Leeds–Lyon Symposium on *Tribology: lubricants and lubrication*, 1995, vol. 30, pp. 513–523. Tribology series (Elsevier, Amsterdam).

82 **Boedo, S.** and **Booker, J. F.** Surface roughness and structural inertia in a mode-based mass-conserving elastohydrodynamic lubrication model. *J. Tribol.*, 1997, **119**(2), 449–455.

83 **Patir, N.** and **Cheng, H. S.** An average flow model for determining effects of three dimensional roughness on partial hydrodynamic lubrication. *ASME J. Lubr. Technol.*, 1978, **100**, 12–18.

84 **Boedo, S.** and **Booker, J. F.** A mode based elastohydrodynamic lubrication model with elastic journal and sleeve. *J. Tribol.*, 2000, **122**(1), 94–102.

85 **Bonneau, D., Guines, D., Frene, J.,** and **Toplosky, J.** EHD analysis including structural inertia effects and a mass-conserving cavitation algorithm. *ASME J. Lubr. Technol.*, 1995, **117**, 540–547.

86 **Murty, K. G.** Note on Bard-type scheme for solving the complementarity problem. *Opsearch*, 1975, **11**, 123–130.

87 ESI Group. *CFD-ACE+ V2006 Modules Manual 2006* (Ed. Huntsville), (ESI CFD, ESI North America, Inc., Alabama).

88 **Campbell, J.** Report TIM 16, 1970 (Glacier Metal Co. Ltd, Birmingham, UK).

89 **Blok, H.** Thermal Instability of flow in elastohydrodynamic films as a cause for cavitation collapse and scuffing. In *Cavitation and related phenomena in lubrication* (Eds D. Dowson, M. Godet, and C. M. Taylor), Proceedings of the 1st Leeds–Lyon Symposium on *Tribology*, University of Leeds, Leeds, UK, 1974, pp. 189–197 (Mechanical Engineering Publications Ltd, London, UK).

90 **Makenham, P. M.** *Investigation of cavitation in a reversed parallel stepped slider bearing*. Master of Science Project (Tribology), University of Leeds, 1968.

91 **Braun, M. J.** and **Hendricks, R. C.** An experimental investigation of the vaporous/gaseous cavity characteristics of an eccentric journal bearing. *ASLE Trans.*, 1984, **27**(1), 1–14.

92 **Etsion, I.** and **Ludwig, L. P.** Observation of pressure variation in the cavitation region of submerged journal bearings. *J. Lubric. Technol.*, 1982, **104**(2), 157–163.

93 **Groper, M.** and **Etsion, I.** The effect of shear flow and dissolved gas diffusion on the cavitation in a submerged journal bearing. *ASME J. Tribol.*, 2001, **123**, 494–500.

94 **Groper, M.** and **Etsion, I.** Reverse flow as a possible mechanism for cavitation pressure build-up in a submerged journal bearing. *ASME J. Tribol.*, 2002, **124**, 320–326.

95 **Heshmat, H.** and **Pinkus, O.** Performance of starved journal bearings with oil ring lubrication. *ASME J. Tribol.*, 1985, **107**, 23–32.

96 **Hays, D. F.** and **Feiten, J. B.** Cavitation between moving parallel plates. In Proceedings of the Symposium *on Cavitation in real liquids*, 1962, pp. 122–138 (GM Research Labs, Warren, Michigan; Elsevier Publishing Co., New York)

97 **Berthe, D.** Cavitation and film rupture in a lubricated contact and its relation to surface degradation. In *Cavitation and related phenomena in lubrication*, Proceedings of the 1st Leeds–Lyon Symposium on *Tribology*, University of Leeds, Leeds, England, 1974, pp. 185–188 (Mechanical Engineering Publications Ltd, London, UK).